

COSMIC RAY ACCELERATION AT RELATIVISTIC AND ULTRARELATIVISTIC SHOCK WAVES

Janusz Bednarz

Jagiellonian University Astronomical Observatory

Ph.D. thesis
written under the supervision of
Dr. hab. Michał Ostrowski

Cracow
November 1999

ACKNOWLEDGMENTS

I am deeply grateful to the supervisor of my thesis Dr. hab. Michał Ostrowski for his guidance and support and, the advice of a number of colleagues and collaborators including Krzysztof Chyży, Włodzimierz Godłowski, Zdzisław Golda, Jacek Guzik, Marek Jamrozy, Jacek Knapik, Tomasz Kobak, Tomasz Kundera, Krzysztof Maślanka, Adam Michalec, Grzegorz Michałek, Katarzyna Otmianowska-Mazur, Stanisław Ryś, Grażyna Siemieniec-Oziębło, Marian Soida, Marek Szydłowski, Bogdan Wszołek and Stanisław Zola from the Cracow Astronomical Observatory were helpful during my work. The presented computations were partly done on a CONVEX Exemplar SPP1000/XA-16 and HP Exemplar S2000 at ACK ‘CYFRONET’ in Kraków. Several parts of the work were supported by Komitet Badań Naukowych through grants PB 1117/P03/94/06, PB 179/P03/96/11 and PB 258/P03/99/17.

Contents

1	Introduction	3
2	Numerical simulations	10
2.1	Acceleration time scale in nonrelativistic versus relativistic shock waves	11
2.2	Transport of particles	13
2.3	Magnetic field	17
2.4	Fitting the spectrum and the acceleration time	18
3	The acceleration time scale in relativistic shock waves	21
3.1	Parallel shocks	21
3.2	Variation of $T_{acc}^{(c)}$ with magnetic field inclination	22
3.3	Variation of $T_{acc}^{(c)}$ with varying turbulence levels	24
4	Ultrarelativistic shock waves	28
4.1	Acceleration mechanism	28
4.2	Energy spectra	29
4.3	The acceleration time scale	34
4.4	The acceleration through particle reflection	39
5	Summary	42
6	Bibliography	44

Chapter 1

Introduction

Ever since the discovery of radiation which comes from cosmos by Hess in 1912 and christened by Millikan in 1925 as ‘cosmic rays’, physicists and astronomers have speculated upon their origin. Fermi (1949) made the first serious attempt at explaining the power law nature of the cosmic ray spectrum. He noted that a particle could increase its energy at collisions against magnetic field irregularities. In his model cosmic rays interact with galactic molecular clouds that move randomly. Particles increase their energy in head-on collisions which are more frequent than overtaking collisions when they loose energy. The process is known as the second-order Fermi acceleration because the mean particle momentum gain $\Delta p/p$ in one interaction is proportional to $(V/v)^2$, V is the root-mean-square velocity of a cloud and v is the particle velocity, considered below to be comparable to the speed of light $- c$. Presently the second-order Fermi acceleration is considered in plasma where the magnetic field fluctuations play a role of the Fermi ‘clouds’.

Nonrelativistic shocks. The concept that shock waves accelerate particles in a mechanism similar to the one described by Fermi (1949) appeared in four seminal papers: Krymski (1977), Axford et al. (1977), Bell (1978a,b) and Blandford & Ostriker (1978). The idea was foreshadowed by Hoyle (1960) who postulated that shocks could efficiently accelerate particles but without specifying a mechanism. Parker (1958) and Hudson (1965, 1967) attempted to obtain such mechanism based on pairs of converging shocks and, most notably, Schatzman (1963) constructed a theory based on perpendicular shocks. Contrary to the original mechanism in the convergent shock flow pattern particles interact with the flowing plasma only like in head-on collisions. Mean momentum gain in such interaction is proportional to U_1/c (U_1 is the shock velocity) and hence the process is known as the first-order Fermi acceleration. Efficiency of the first-order relative to the second-order Fermi acceleration equals roughly U_1/V_A , where V_A is the Alfvén speed in plasma (cf. Ostrowski & Schlickeiser 1996).

A shock wave, or briefly a shock, can be described as a sharp transition layer which propagates through plasma with a velocity exceeding the speed of sound and changes its state through the compression. The thickness of the layer is determined

by the physical process responsible for thermodynamic parameters transfer from incoming plasma, upstream of the shock, to flowing away plasma, downstream of the shock. In tenuous plasma the transfer proceeds through collective electromagnetic effects and the shock width is of the order of the gyroradius of a thermal ion. In the acceleration process we will consider relativistic particles which move with speeds close to the speed of light and have a gyroradii much larger than thermal ions and consequently they see the shock as a discontinuity.

The acceleration processes in nonrelativistic – $U_1 \ll c$ – shocks yield power-law particles momentum spectra, $f(p) \propto p^{-\alpha}$, with a very simple formula for the spectral index of accelerated particles

$$\alpha = \frac{3r}{r-1} \quad , \quad (1.1)$$

where

$$r = \frac{\gamma_a + 1}{\gamma_a - 1 + 2M^{-2}} \quad (1.2)$$

is a shock compression ratio, M is the shock Mach number and γ_a is the plasma adiabatic index. For a strong shock, $M \rightarrow \infty$, propagating in a nonrelativistic plasma with $\gamma_a = 5/3$ we have $r \rightarrow 4-$ and $\alpha \rightarrow 4+$. This is encouragingly close to the index of 4.3 inferred for the source of the galactic cosmic rays. Similarly, the acceleration time expressed by a simple diffusive formula is discussed in Section 3.

Relativistic shocks. A consistent method to tackle the problem of first-order Fermi acceleration in relativistic shock waves was conceived by Kirk & Schneider (1987a; see also Kirk 1988). They assumed a parallel shock geometry and that particles are subject to pitch-angle scattering on each side of the shock. By extending the diffusion approximation to higher order terms in the anisotropy of the particle distribution, they obtained solutions to a kinetic equation of the Fokker–Planck type with the isotropic form of pitch angle diffusion coefficient. Since pitch-angle scattering conserves the particle momentum in the fluid frame, the energy spectrum is obtained by matching the solutions at the shock. Their Q_L method yielded a particle energy spectral index for strong nonrelativistic shocks as $\sigma \simeq 2.0$ – where $\sigma \equiv \alpha - 2$ – in agreement with previous results. For relativistic shocks with realistic compression of Heavens & Drury (1988), the method produced particle spectra with σ slightly smaller than 2 provided the Lorentz factor of the shock $\gamma \leq 5$, and slightly larger at higher γ . The authors derived also an angular distribution function at the shock as measured in the upstream and the downstream fluid frame. In the upstream fluid frame the distribution is strongly peaked even for a mildly relativistic case of $U_1 = 0.3c$.

Next, Kirk & Schneider (1988) extended the analysis by involving both diffusion and large-angle scattering in particle pitch angle. They discovered that – in relativistic shock waves – the presence of large angle scattering can substantially modify the spectrum of accelerated particles. An extension of the Kirk & Schneider's (1987a) approach to more general conditions in the shock was given by Heavens & Drury (1988) who took into consideration the fluid dynamics of relativistic shock

waves. They also noted that the resulting particle spectral indices depend on the perturbations spectrum near the shock in contrast to the nonrelativistic case.

Kirk & Heavens (1989) considered the acceleration process in shocks with magnetic fields oblique to the shock normal (see also Ballard & Heavens 1991) by extending the method of Kirk & Schneider (1987a). Oblique shock fronts may be conveniently classified into two categories: subluminal and superluminal. In the former ones it is possible to find a Lorentz transformation to a frame of reference in which the electric field is zero in both the upstream and the downstream regions, and the shock front is stationary. In this frame, called the de Hoffman-Teller frame (de Hoffman & Teller 1950), the energy of a particle remains constant provided it does not suffer scattering. Superluminal shocks, however, do not admit a transformation to such a frame of reference. They correspond to shock fronts in which the point of intersection of the front with a magnetic field line moves at a speed greater than c . Kirk & Heavens used the de Hoffman-Teller frame to consider the subluminal shocks. They showed, contrary to nonrelativistic results again, that such shocks led to flatter spectra than parallel ones approaching the value $\sigma \simeq 1.0$ when the shock velocity along the magnetic field $U_B \simeq c$. Their work relied on the assumption of adiabatic invariant p_\perp^2/B conservation for particles interacting with the shock, which restricted considerations to the case of a nearly uniform magnetic field upstream and downstream of the shock.

A different approach to particle acceleration was presented by Begelman & Kirk (1990) who noted that in relativistic shocks most field configurations lead to superluminal conditions for the acceleration process. In such conditions, particles are accelerated in a single shock transmission by drifting parallel to the electric field present in the shock. Begelman & Kirk showed that there is more efficient acceleration in relativistic conditions than that predicted by a simple adiabatic theory.

The acceleration process in the presence of finite amplitude magnetic field perturbations was considered by Ostrowski (1991; 1993) and Ballard & Heavens (1992). Ostrowski considered a particle acceleration process in the relativistic shocks with oblique magnetic fields in the presence of field perturbations, where the assumption $p_\perp^2/B = \text{const}$ was no longer valid. To derive particle spectral indices he used a method of particle Monte Carlo simulations and noted that the spectral index was not a monotonic function of the perturbation amplitude enabling the occurrence of steeper spectra than those for the limits of small and large perturbations. It was also revealed that conditions leading to very flat spectra involve an energetic particle density jump at the shock. The acceleration process in the case of a perpendicular shock shows a transition between the compressive acceleration described by Begelman & Kirk (1990) and, for larger perturbations, the regime allowing for formation of the wide range power-law spectrum. The Ostrowski (1991) method was based on the ‘mean field + perturbation’ decomposition of magnetic field, i.e. a particle is considered to propagate in the mean field along its undisturbed ‘adiabatic’ trajectory, while the magnetic field inhomogeneities are allowed for by perturbing the trajectory parameters in finite time-steps. The simulations of Ostrowski (1993)

were based on the numerical integration of the particle equations of motion in a perturbed magnetic field. Finite-amplitude field perturbations were described with analytic formulae as a superposition of static sinusoidal waves.

The analogous simulations by Ballard & Heavens (1992) for highly disordered background magnetic fields show systematically steeper spectra in comparison to the above results, as discussed by Ostrowski (1993). In terms of the Lorentz factor of the shock Ballard & Heavens found a rough relation $\alpha \simeq (3\gamma + 1)/8$ that is valid up to $\gamma \simeq 5$. They checked their results considering different power-law fluctuations spectra for the magnetic field and stated that differences between the resulting particle spectra were quite small.

The particle spectrum formation in the presence of non-linear coupling of accelerated particles to the plasma flow has been commented by Ostrowski (1994).

The shock waves propagating with relativistic velocities rise also interesting questions concerning the cosmic ray acceleration time scale, T_{acc} . Until our results published in 1996 (Bednarz & Ostrowski 1996 - see chapter 3) there was only somewhat superficial information available about that problem. A simple comparison to the nonrelativistic formula based on numerical simulations shows that T_{acc} relatively decreases with increasing shock velocity for parallel (Quenby & Lieu 1989; Ellison et al. 1990) and oblique (Takahara & Terasawa 1990; Newman et al. 1992; Lieu et al. 1994; Quenby & Drolias 1995; Naito & Takahara 1995) shocks. However, the numerical approaches used there, based on assuming the particle isotropization at each scattering, neglect or underestimate a significant factor controlling the acceleration process – the particle anisotropy. Ellison et al. (1990) and Naito & Takahara (1995) included also derivations applying the pitch angle diffusion approach. The calculations of Ellison et al. for parallel shocks show similar results to the ones they obtained with large amplitude scattering. In their computations for the shock with velocity $0.98c$ the acceleration time scale is reduced on a factor ~ 3 with respect to the nonrelativistic formula. Naito & Takahara considered shocks with oblique magnetic fields. They confirmed the reduction of the acceleration time scale with increasing inclination of the magnetic field derived earlier for nonrelativistic shocks (Ostrowski 1988). However, their approach neglected the effects of particle cross field diffusion and assumed the adiabatic invariant conservation at particle interactions with the shock. These two simplifications limit their results to the cases with small amplitude turbulence near the shock¹. One should also note that comparing some of the mentioned papers the derived time scales to the nonrelativistic expression does not have any clear physical meaning when dealing with relativistic shocks.

In the present paper we use pitch angle diffusion approximation for particle transport in the acceleration process. Let us note that some earlier derivations of the acceleration time scale were based on the numerical simulations involving particle

¹One should note that the spatial distributions near the shock derived by these authors (their figures 1 and 2) do not show a particle density jump proved to exist in oblique relativistic shocks by Ostrowski (1991). It is also implicitly present in analytic derivations of Kirk & Heavens (1989).

scattering at point like scattering centers isotropizing the particle momentum at each scattering, the so called large angle scattering model. This approach does not provide a proper description for the acceleration processes in shock waves moving with velocities comparable to the particle velocity because it removes particle anisotropy and changes the factors related to it. Moreover, against arguments presented in some papers such scattering patterns can not be realized in turbulent magnetic fields near relativistic shocks, where most particles active in the acceleration process are able to diffuse only a short distance below a few particle gyroradii off the shock². Such distances are most often insufficient to allow for big particle pitch-angle changes. In shocks with oblique magnetic fields such large angle scattering patterns can substantially change the shape of the accelerated particle spectrum with respect to the pitch angle diffusion model. Additionally, as an individual particle interaction with the shock can involve a few revolutions along the magnetic field, the usually assumed adiabatic invariant conservation, $p_{\perp}^2/B = \text{const}$, cannot be valid for short inter-scattering intervals.

Ultrarelativistic shocks. The acceleration mechanism described in section 4.1 is quite different from that in the nonrelativistic and mildly relativistic regime so that we distinguish a class of ultrarelativistic shocks if their Lorentz factors $\gamma \gg 1$. The condition $\gamma \gg 1$ implies also some simplifications that allow to consider ultrarelativistic shocks as a separate class. First, the magnetic field inclination downstream of the shock is, in practice, always perpendicular to the shock normal as one can derive from Eq. 2.14. Similarly, we can approximate in Eq. 2.13 the ratio of the value the magnetic field downstream of the shock to upstream as $B_2/B_1 \simeq \sqrt{8\gamma} \sin \psi_1$. A turbulence downstream of the shock could amplify this value and for example assuming equipartition with the thermal pressure downstream, one obtains $B_2/B_1 \sim (c/V_A)\gamma$. Moreover, independently of the plasma composition (proton-electron or electron-positron) the shock velocity relative to the downstream medium is $U_2 = c/3$ in the limit of large γ .

The ultrarelativistic shocks are characterized by large anisotropy of particle momentum distribution near the shock that was presented in Bednarz & Ostrowski (1998, see Figs. 4.4 - 4.7 below). The values of two main parameters describing the acceleration process, namely the energy spectral index and the acceleration time, are independent of shock conditions if fluctuations upstream of the shock ensure the acceleration process to be effective. They tend to 2.2 (spectral index, Bednarz & Ostrowski 1998; also Bednarz & Ostrowski 1997a,b) and 1.0 r_g/c (acceleration time, Bednarz 1998, 1999). The rough analytical calculations of Gallant & Achterberg (1999) are consistent with the Bednarz & Ostrowski (1998) paper and Gallant et al. (1998) confirm the value of spectral index for the specific condition of the extremely disordered magnetic field downstream of the shock.

Ultrarelativistic shocks are considered as sources of cosmic rays with energies exceeding 10^{20} eV and several papers suggested that gamma ray bursts (GRBs) could

² However, for the nonrelativistic shock velocity and particles much above the injection energy such approximations can be safely used (cf. Jones & Ellison 1991).

be sources of these particles (cf. Waxman 1995, Vietri 1995). Vietri (1995) argued that in the Fermi-type acceleration at an ultrarelativistic shock, a particle could have an relative energy gain $\sim \gamma^2$ per shock crossing cycle. Gallant & Achterberg (1999) showed that particles with initial momenta isotropically distributed upstream of the shock gain $\sim \gamma^2$ energy, but only at the first interaction of the shock. They also showed that for parameters typical of the millisecond pulsars in the neutron star binaries observed in our Galaxy, the gamma ray burst blast wave would decelerate within the pulsar wind bubble, yielding an energy spectrum $\sigma \simeq 2$ for the boosted particles. Moreover, this spectrum would typically extend over the energy region $10^{18.5} - 10^{20}$ eV, i.e. precisely where the ultra-high-energy cosmic rays (UHECR) component is observed. Bednarz (1999) suggested that such extremely energetic particles could be produced by reflections of the shock directly in GRBs.

Relativistic shocks in astrophysical objects. Results presented further in the theses could be applied in models of some galactic and extragalactic objects. One of those are active galactic nuclei where a central black hole ejects plasma in the form of relativistic jets. A few tens of blazars has been detected in GeV γ -rays by the EGRET detector (von Montigny et. al. 1995). It is widely believed that the γ -ray production in blazars is strictly related to the existence of relativistic jets because many of them show superluminal motions (Vermeulen & Cohen 1994). Jiang et al. (1998) applied the Königl inhomogeneous jet model (Blandford & Königl 1979; Königl 1981) to a sample of quasars and BL Lacs objects and found the Lorentz factors of jets to be a significant part the ultrarelativistic ones. In unified schemes for active galactic nuclei the Fanaroff-Riley type II (FR II) radio sources are formed by AGNs, similarly to blazars, but jets are ejected at higher angles to the line of sight. Evidence that they are relativistic even on tens or hundreds kiloparsec scales suggest that the hotspots in these sources are the downstream regions of relativistic shocks.

The recent finding of microquasars in our Galaxy, a class of objects that mimic – on scales million of times smaller – the properties of quasars opened new possibilities to study physical processes in accretion disks of black holes. The observations of Mirabell & Rodriguez (1994), Tingay et al. (1995), and Hjellming & Rupen (1995) confirm the existence of relativistic flows related to these objects, and it is expected that they form relativistic shocks in the interstellar medium.

A relativistic wind of magnetized electron-positron plasma blowing from a pulsar with the flow Lorentz factor of $\sim 10^6$ is expected to form a termination shock (e.g. Kennel & Coroniti 1984; Gallant & Arons 1994 and Chiueh et al. 1998). Non-thermal radiation apparently seen in the class of such objects – plerions – suggests the existence of acceleration processes inside the nebula. The Crab Nebula as the young and energetic source is the best plerion to study it. Recent optical observations of Crab Nebula using the Hubble Space Telescope and also the X-ray observations of ROSAT (cf. Hester et al. 1995) show a fascinating structure of jets, a torus of X-ray emission and complexes of sharp wisps. γ ray observations of the Crab Nebula exhibit the existence of extremely energetic electrons near the pulsar

(cf. de Jager et al. 1996). The electron energy is a few magnitudes larger than that in the blowing wind so an acceleration mechanism has to take place near the pulsar. Gallant & Arons (1994) proposed a mechanism where electrons gain their energy from electromagnetic waves generated by gyrating ions. The mechanism tries to explain wisps at the distance of $10''$ from the pulsar but a knot found at $0.7''$ (cf. Hester et al. 1995) is not explained in the model. We expect that acceleration mechanism presented by Bednarz & Ostrowski (1998) and Bednarz (1999) is able to account for the generation of such energetic electrons at if the ultrarelativistic shock formed near the pulsar.

Observations carried out by the Burst and Transient Source Experiment show that GRBs originate from cosmological sources (Meegan et al. 1992 and Dermer 1992). Identification of the host galaxy for the GRB 971214 (Kulkarni et al. 1998) and several other bursts causes there is little doubt now that some, and most likely all GRBs are cosmological. These phenomena are surely related to ultrarelativistic shocks with $\gamma > 10^2$ (cf. Woods & Loeb 1995). The power-law form of the spectrum often observed at high photon energies suggests the existence of nonthermal populations of energetic particles. Bednarz & Ostrowski (1998, see chapter 4 below) showed that such shocks are able to accelerate charged particles and values of their energy spectral indices converge to $\sigma = 2.2$ when $\gamma \rightarrow \infty$ and/or the magnetic turbulence amplitude grows.

Below, we will present our results on relativistic shock acceleration published in a series of papers Bednarz & Ostrowski (1996, 1998, 1999) and Bednarz (1999). In the next chapter we discuss our numerical simulations and problems with their application to relativistic shock conditions. Then, in chapter 3, the acceleration time scales in mildly relativistic shocks are derived for a number of magnetic field configurations. Chapter 4 is devoted to ultrarelativistic shocks. We show convergence of the particle energy spectral index to the asymptotic value $\sigma_\infty \simeq 2.2$ for $\gamma \rightarrow \infty$. We also discuss particle reflections from large γ shocks providing a limit for models involving GRBs as sources of UHECR. The acceleration time scale is also derived. In the last chapter 5 a short summary is presented.

Chapter 2

Numerical simulations

In order to consider the role of particle anisotropic distributions and different configurations of the magnetic field in shocks the present work is based on the small angle particle momentum scattering approach described by Ostrowski (1991). It enables us to model effects of cross-field diffusion, important in shocks with oblique magnetic fields. Let us note (cf. Ostrowski 1993) that this code allows for a reasonable description of particle transport in the presence of large amplitude magnetic field perturbations also.

Some earlier derivations of the acceleration time scale were based on the numerical simulations involving particle scattering at point like scattering centers isotropizing the particle momentum at each scattering. This approach does not provide a proper description for the acceleration processes in shock waves moving with velocities comparable to the particle velocity because it removes particle anisotropy and changes factors related to it. Moreover, against arguments presented in some papers, such scattering pattern can not be realized in turbulent magnetic fields near relativistic shocks, where most particles active in the acceleration process are able to diffuse only a short distance below a few particle gyroradii off the shock¹. Such distances are often insufficient to allow for big particle pitch-angle changes occurring with the *point-like* scattering centers which isotropize particle momentum at each scattering. In shocks with oblique magnetic fields such scattering pattern can substantially change the shape of the accelerated particle spectrum with respect to the pitch angle diffusion model. Additionally, as an individual particle interaction with the shock can involve a few revolutions along the magnetic field, the usually assumed adiabatic invariant conservation, $p_{\perp}^2/B = \text{const}$, cannot be valid for short inter-scattering intervals.

Below, the light velocity is used as the velocity unit, $c = 1$. As the considered particles are ultrarelativistic ones, $p = E$, we often put the particle momentum for its energy. In the shock we label all upstream (downstream) quantities with the subscript ‘1’ (‘2’). The quantities are given in their respective plasma rest frames

¹ However, for the nonrelativistic shock velocity and particles much above the injection energy such approximation can be safely used (cf. Jones & Ellison 1991).

but subscripts U or D mean that a parameter is measured in upstream plasma rest frame or downstream plasma rest frame, respectively.

The shock normal rest frame is the one with the plasma velocity normal to the shock, both upstream and downstream the shock (cf. Begelman & Kirk 1990). The acceleration time scales in relativistic shocks (chapter 3), T_{acc} , are always given in this particular frame in units of the upstream gyroradius divided by c but the downstream plasma rest frame quantities are used (chapter 4) for the case of ultra-relativistic ones, t_{acc} .

Here we affix a gyroradius with the index ‘g’ when it is a value given for the local *uniform* (tantamount to *mean* or *homogeneous*) magnetic field component. Index ‘e’ means the *effective* field including the field perturbations (see Eq. 2.15).

Let us denote parallel diffusion coefficient as κ_{\parallel} and perpendicular diffusion coefficient as κ_{\perp} . Moreover, we will sometimes use shortcuts $\tau \equiv \kappa_{\perp}/\kappa_{\parallel}$ and $\lambda \equiv \log_{10}(\kappa_{\perp}/\kappa_{\parallel})$.

If it will not cause ambiguity we will use symbol ψ to designate the magnetic field inclination to the shock normal upstream of the shock, instead of ψ_1 , and the Lorentz factor of the shock as seen upstream of the shock as γ , instead of γ_1 . For the same magnetic field fluctuation patterns upstream and downstream of the shock we will use symbols without indices for these patterns.

2.1 Acceleration time scale in nonrelativistic versus relativistic shock waves

In the case of a nonrelativistic shock wave, with velocity $U_1 \ll 1$, the acceleration time scale can be defined as

$$T_{acc} \equiv \frac{E}{\overline{\Delta E}} \quad , \quad (2.1)$$

where $\overline{\Delta E}$ is the mean energy gain at particle interaction with the shock and Δt is the mean time between successive interactions. One can use mean values here because any substantial increase of particle momentum requires a large number of shock-particle interactions and the successive interactions are only very weakly correlated with each other. The respective expression for T_{acc} in parallel shocks,

$$T_{acc}^0 = \frac{3}{U_1 - U_2} \left\{ \frac{\kappa_1}{U_1} + \frac{\kappa_2}{U_2} \right\} \quad , \quad (2.2)$$

where κ_i is the respective particle spatial diffusion coefficient, has been discussed by Lagage & Cesarsky (1983). Ostrowski (1988) provided the analogous scale for shocks with oblique magnetic fields and small amplitude magnetic field perturbations. It can be written in the form

$$T_{acc}^{\psi} = \frac{3}{U_1 - U_2} \left\{ \frac{\kappa_{n,1}}{U_1 \sqrt{\frac{\kappa_{n,1}}{\kappa_{\parallel,1} \cos^2 \psi_1}}} + \frac{\kappa_{n,2}}{U_2 \sqrt{\frac{\kappa_{n,2}}{\kappa_{\parallel,2} \cos^2 \psi_2}}} \right\} \quad , \quad (2.3)$$

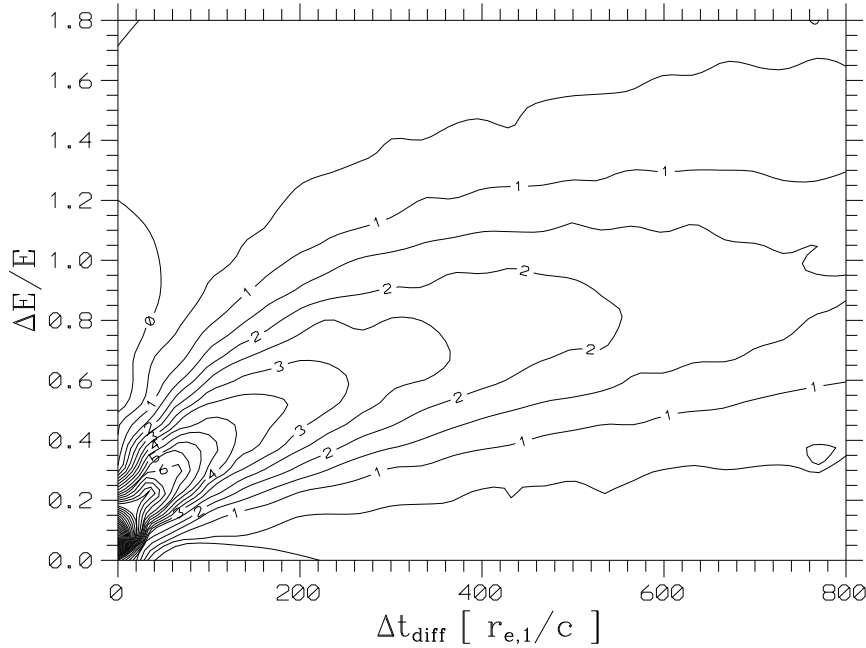


Figure 2.1: Distribution of particle-shock interaction events for upstream particles, $N(\Delta t_{diff}, \Delta E/E)$, in function of the upstream diffusive times, Δt_{diff} , and the respective energy changes, $\Delta E/E$. The correlation between Δt_{diff} and $\Delta E/E$ is represented by a regular drift of the distribution maximum toward higher $\Delta E/E$ when increasing Δt_{diff} . An example for the parallel shock with $U_1 = 0.5$, $\psi_1 = 1^\circ$ and weak scattering conditions ($\kappa_\perp/\kappa_\parallel = 1.6 \cdot 10^{-6}$) is presented.

where the index n denotes quantities normal to the shock, the index \parallel those parallel to the magnetic field, ψ is an angle between the magnetic field and the shock normal and $U_1/\cos\psi_1 \ll c$ is assumed. The terms $\sqrt{\kappa_n/(\kappa_\parallel \cos^2\psi)}$ represent a ratio of the mean normal velocity of a particle to such velocity in the absence of cross-field diffusion. One may note that for negligible cross-field diffusion the expression (2.3) coincides with (2.2) if we put $\kappa_{n,i}$ for κ_i ($i = 1, 2$). The case of oblique shock with finite amplitude field perturbations has not been adequately discussed yet, but we expect the respective acceleration scale to be between the values given by the above formulae for T_{acc}^0 and T_{acc}^ψ . The influence of the particle escape boundary on the acceleration time scale and the particle spectrum is discussed by Ostrowski & Schlickeiser (1996).

If the shock velocity becomes relativistic, the particle energy change at a single interaction with the shock can be comparable, or even larger than the original energy. Moreover, after interaction with the shock, the *upstream* particles with small initial angles between its momenta and the mean magnetic field have a larger chance to travel far away from the shock. On average, such particles spend longer times and are able to change its pitch angles substantially until the next hits at the shock. Then, larger pitch angles allow for particle reflections with large energy gains or for transmissions downstream (cf. Ostrowski 1991, Lucek & Bell 1994). Therefore,

correlations of the times between successive interactions, Δt_{diff} , the energy gains at these interactions, ΔE , and possibly the probability of particle escape occur. As an example, in Fig. 2.1 we map the number of particle interactions with the shock in coordinates $(\Delta t_{diff}, \Delta E)$. A cut of the presented surface at any particular value of Δt_{diff} gives the distribution of energy gains for particles who have spent this time since the last interaction with the shock. A general trend seen on the map for increasing Δt_{diff} is the growing value of $\Delta E/E$ for the distribution maximum. Because of these correlations are accompanied with the large energy gains $\Delta E \sim E$, we propose a different approach to the derivation of the acceleration time scale with respect to the one used for nonrelativistic shocks. Usually the acceleration time scale is applied for the derivation of the highest energies occurring in the particle spectrum, characterized by its cut-off energy, E_c . Thus we use this energy scale to define the acceleration time scale as

$$T_{acc}^{(c)} \equiv \frac{E_c}{\dot{E}_c} \quad , \quad (2.4)$$

where $\dot{E}_c \equiv dE_c/dt$. The rate of the cut-off energy increase is a well-defined quantity and the time scale (2.4) has a clear physical interpretation. The above definition does not require any limit for the energy gains of individual particles and all possible correlations are automatically included here. From the meaning of the definition (2.4) it follows that $T_{acc}^{(c)}$ is somewhat shorter than the respective scale at the same energy for later times required for the respective part of the spectrum to become a pure power-law (cf. Ostrowski & Schlickeiser 1996). One should also note that in relativistic shocks the time scale depends on the reference frame we use for its measurement. In the present paper the acceleration time scales are given in the respective normal shock rest frame. However, the applied time units $r_{e,1}/c$ are defined with the use of the upstream gyration time.

2.2 Transport of particles

To derive particle trajectories in a disturbed magnetic field one should, in general, integrate full equation of motion along these trajectories (see summary in Decker 1988 and Ostrowski 1988). However, for slightly inhomogeneous fields it was proposed a ‘quasi-linear’ approximation for analytical calculations (e.g. Jokipii 1971) consisting of distinguishing between two factors determining a particle’s trajectory: the ‘adiabatic’ undisturbed motion in the mean field \vec{B}_0 , and perturbations to this trajectory derived by averaging the effect of magnetic field perturbations $\delta\vec{B} = \vec{B} - \vec{B}_0$ along the trajectory. As a result the description of particle transport in terms of the Fokker-Planck equation includes the diffusive term in the pitch angle ϑ , where $\vartheta \equiv \angle(\vec{p}, \vec{B}_0)$, which describes trajectory perturbations and all quantities are averaged over the phase angle along the trajectory φ . In the case of efficient particle scattering maintaining the particle distribution function $f(\vec{r}, p, \vartheta, t)$ is very nearly

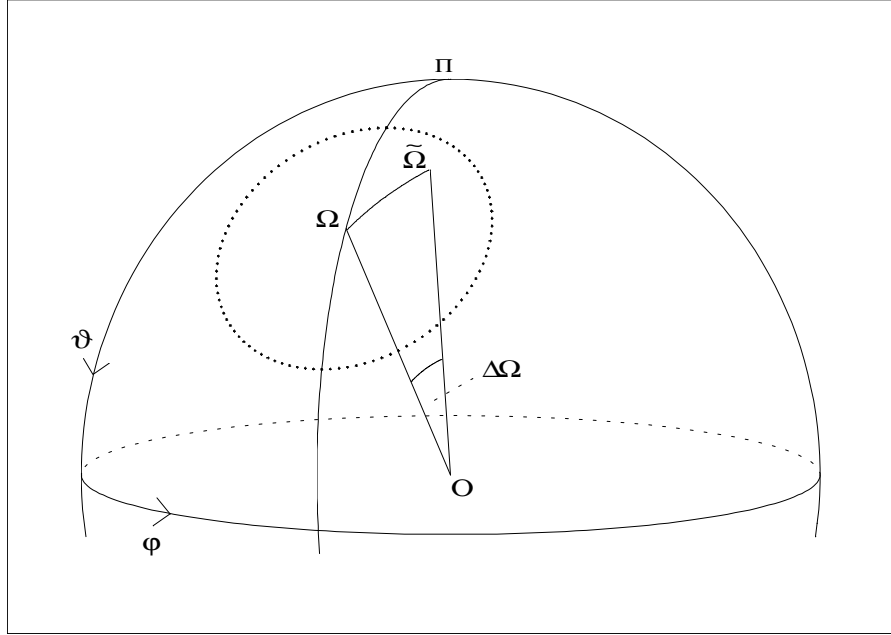


Figure 2.2: Particle momentum scattering at the sphere $|\vec{p}| = \text{const.}$ The sphere is parameterized with coordinates ϑ and φ . A particle with the original momentum pointing towards Ω with coordinates (ϑ, φ) is scattered to a point $\tilde{\Omega}$ with coordinates $(\vartheta_{\text{new}}, \varphi_{\text{new}})$, within a circle at the sphere with radius $\Delta\Omega_{\text{max}}$. The scattering angle is $\Delta\Omega \equiv \angle(\Omega O \tilde{\Omega})$ and the scattering azimuthal angle $\beta \equiv \angle(\Pi \Omega \tilde{\Omega})$.

isotropic, the equation can be reduced to the spatial diffusion equation. Concerning the pitch angle diffusion, all information on the particle scattering process is contained in the pitch angle diffusion coefficient $D_\vartheta = \langle \Delta\vartheta^2 \rangle / (2\langle \Delta t \rangle)$ where $\Delta\vartheta$ ($\ll 1$) is the change of ϑ during an individual ‘scattering act’, and $\langle \dots \rangle$ denotes taking the average (see Chandrasekhar 1943). Perturbing force acts at the particle trajectory in a continuous way, and the notion of the scattering act may be introduced by summing up all changes to the orbit over some time Δt , long enough for the corresponding pitch angle changes to be uncorrelated in the successive scattering acts. In applications, usually a process of diffusion in parameter $\mu \equiv \cos\vartheta$ with the corresponding diffusion coefficient, $D_\mu = D_\vartheta(1 - \mu^2)$ is considered. The relation of the above Fokker-Planck approach to the general situation also involving large-angle scattering was discussed by Kirk & Schneider (1988). Our numerical approach resembles the one applied by Kirk & Schneider (1987b).

We restrict our consideration to the test-particle approximation, in which it is assumed that particles are scattered by scattering centers in the fluid but have no effect either on the fluid velocity or on the density of scattering centers. Between two successive scatterings, the particle is assumed to proceed along the undisturbed path in the mean field. We will furthermore assume that the scattering centers are frozen into the fluid. The assumption implicates that $|\vec{p}| = \text{const.}$ We introduce discrete uncorrelated perturbations of the particle’s direction [i.e. perturbations in $\Delta\vartheta$ (or

$\Delta\mu)$ and $\Delta\varphi]$, in finite time steps, Δt . Thus, all particle momentum vectors can be represented as points on the sphere of constant $|\vec{p}|$ parameterized with two angles ϑ (or μ) and φ (Fig. 2.2). All our calculations were performed in the respective local plasma rest frame. In any such frame the electric field vanishes and particle energies are conserved.

If the distribution of the particle orientation $\Omega \equiv (\vartheta, \varphi)$ at the sphere (Fig. 2.2) maintain the same form at any point on that sphere independently of the local coordinate lines then the scattering process is not affected by the orientation. In the case one gets ‘isotropic’ diffusion coefficient D_ϑ that is independent of ϑ . Let us denote the scattering amplitude (angle between the original orientation Ω and the one after scattering $\tilde{\Omega}$) as $\Delta\Omega$, and the angle between the meridian, $\varphi = \text{const}$, and the great circle connecting Ω with $\tilde{\Omega}$ as β . For consistency we demand that, in the limit of small scattering amplitudes, the considered scattering model should lead to an isotropic diffusion coefficient. The considered scattering probability distribution, $F = F(\Delta\Omega, \beta)$ must satisfy the ‘elliptical’ symmetry: $F(\Delta\Omega, \beta) = F(\Delta\Omega, \pi - \beta) = F(\Delta\Omega, -\beta)$. Kirk & Schneider (1987b) used the distribution $F(\Delta\Omega, \beta)$ derived from the heat conduction equation. It was equivalent to assuming that the diffusive character of particle trajectories is also preserved at the limit $\Delta t \rightarrow 0$. However, in a general case, one should assume a form determined by considered form of the magnetic field perturbations. The simple choice is to take $F = F(\Delta\Omega)$ which does not distinguish any direction in space. Unless one has any particular pattern of field perturbations it is the most natural choice and we will restrict ourselves to such distributions below. In particular, we take it in a normalized form

$$F(\Delta\Omega) = \begin{cases} (1 - \cos \Delta\Omega_{\max})^{-1} \sin \Delta\Omega & (\Delta\Omega \leq \Delta\Omega_{\max}) \\ 0 & (\Delta\Omega > \Delta\Omega_{\max}) \end{cases} \quad (2.5)$$

which ensures an equal probability of reaching any unit surface element of the sphere within the range $\Delta\Omega_{\max}$ from the original position. One should note that this model scattering is no longer a symmetric one in μ . The fact is visible after averaging the spherical triangle relation (Eq. 2.11) over β , for a given $\Delta\Omega$, the mean change of μ is $\langle \Delta\mu \rangle = \mu(\cos \Delta\Omega - 1)$. The anisotropy results from the projection of the circle $\Delta\Omega = \text{const}$ in the spherical coordinates (μ, φ) and, for constant $\Delta\Omega_{\max}$, does not lead to any actual particle anisotropy. In the Fokker-Planck equation

$$\frac{\partial f}{\partial t} + v\mu \frac{\partial f}{\partial z} = \frac{\partial}{\partial \mu} \left(\frac{\langle \Delta\mu \rangle}{\Delta t} f \right) + \frac{1}{2} \frac{\partial^2}{\partial \mu^2} \left(\frac{\langle \Delta\mu^2 \rangle}{\Delta t} f \right) \quad , \quad (2.6)$$

where $f \equiv f(z, \mu, t)$ is the particle distribution function presented in simplified form with a spatial coordinate z along the magnetic field, any homogeneous stationary solution must be the isotropic one. Thus the consistency condition for the Fokker-Planck coefficients is

$$\langle \Delta\mu \rangle + \frac{1}{2} \frac{\partial}{\partial \mu} \langle \Delta\mu^2 \rangle = 0 \quad , \quad (2.7)$$

and the above mentioned anisotropy is compensated for by a gradient of the diffusion coefficient D_μ .

From the distribution (2.5), for $\Delta\Omega_{max} \ll 1$, one obtains the relation between mean values $2\langle\Delta\Omega^2\rangle \simeq 4\langle\Delta\vartheta^2\rangle \simeq \Delta\Omega_{max}^2$. Using the definition $D_\vartheta \equiv \langle\Delta\vartheta^2\rangle/(2\langle\Delta t\rangle)$, we obtain

$$\Delta\Omega_{max}^2 = 8D_\vartheta\langle\Delta t\rangle \quad . \quad (2.8)$$

A great number of reasonable distributions of Δt could be proposed for any value of $\langle\Delta t\rangle$, which may be interpreted as representative for different perturbations spectra. In the limit of infinitesimal scattering amplitude the physical picture is not sensitive to the particular choice of this distribution. However, for higher amplitudes and anisotropic particle distributions this selection may qualitatively affect the simulation results and should be done with great care (cf. Kirk & Schneider 1987b, 1988). For the simulation of large-amplitude scattering one can use equation (2.8) only in a formal manner. Now, the factor $8D_\vartheta$ still provides the relation between $\Delta\Omega_{max}$ and $\langle\Delta t\rangle$, but for scatterings of small amplitude it has the additional property of being 8 times the pitch angle diffusion coefficient. Let us also note that in our method we make use of the concept of a mean field and assume that the scatterings are not correlated. For highly perturbed magnetic fields both assumptions may be of limited validity.

Based on the above model one is able to construct an algorithm for the derivation of the scattering momentum orientation $(\mu_{new}, \varphi_{new})$ from the original one (μ, φ) , after an individual scattering act. Let us denote two independent random values from the range $(0, 1)$ as R_1 and R_2 . Using equation (2.5) we can generate the value for $\Delta\Omega$ as

$$\cos(\Delta\Omega) = 1 - (1 - \cos\Delta\Omega_{max})R_1 \quad (2.9)$$

and the orientation angle β

$$\beta = 2\pi R_2 \quad . \quad (2.10)$$

The new value for pitch angle cosine is derived from the spherical triangle $\Omega\Pi\tilde{\Omega}$ of Fig 2.2 as

$$\mu_{new} = \mu \cos \Delta\Omega + \sqrt{1 - \mu^2} \sin \Delta\Omega \cos \beta \quad . \quad (2.11)$$

In equation (2.11) an exact value for μ_{new} is obtained, and one can consider high-amplitude scattering ($\Delta\Omega \sim 1$) as well. However, as was mentioned previously, one should consider carefully the meaning of the diffusion coefficient in this case. For instance, in simulating a diffusion perpendicular to the field one should also account for the possibility of phase perturbation along the trajectory. In our approach the considered spherical triangle yields

$$\varphi_{new} = \varphi + \arctan \left(\frac{\sin \Delta\Omega \sin \beta}{\cos \Delta\Omega \sqrt{1 - \mu^2} - \sin \Delta\Omega \mu \cos \beta} \right) + \pi H(\mu\mu_{new} - \cos \Delta\Omega) \quad , \quad (2.12)$$

where $H(x)$ is the Heaviside step function.

2.3 Magnetic field

In the present discussion we consider the role of the mean magnetic field configuration and the amount of particle scattering. In order to avoid effects of varying shock compression due to the presence of different magnetic field configurations we take the field as a trace one without any dynamical effects on the plasma flow. The shock compression, as seen in the shock normal rest frame, $r = U_1/U_2$, is derived from the approximate formulae presented by Heavens & Drury (1988). For illustration of the results, in the present theses we consider the shock waves propagating in the cold electron-proton plasma. For the *mean* magnetic field B_1 taken in the upstream plasma rest frame and inclined at the angle ψ_1 with respect to the shock normal we derive its downstream value and inclination, B_2 and ψ_2 , with the use of jump conditions presented for relativistic shocks by e.g. Appl & Camenzind (1988)

$$B_2 = B_1 \sqrt{\cos^2 \psi_1 + R^2 \sin^2 \psi_1} \quad , \quad (2.13)$$

$$\tan \psi_2 = R \tan \psi_1 \quad , \quad (2.14)$$

where $R = r \gamma_1 / \gamma_2$ and the Lorentz factors $\gamma_i \equiv 1 / \sqrt{1 - U_i^2}$ ($i = 1, 2$). These formulae are valid for both sub- and super-luminal magnetic field configurations.

We model particle trajectory perturbations by introducing small-angle random momentum scattering along the mean-field trajectory (cf. Ostrowski 1991). The particle momentum scattering distribution is uniform within a cone wide at $\Delta\Omega$, along the original momentum direction. The presented simulations for mildly relativistic shocks use a constant value of $\Delta\Omega = 0.173$ ($= 10^\circ$). Scattering events are at discrete instants, equally spaced in time as measured in the units of the respective $r_{g,i}/c$ ($i = 1, 2$). The increasing perturbation amplitude is reproduced in simulations by decreasing the time period Δt between the successive scatterings.

In ultrarelativistic shock waves efficient particle scattering with a very small $\Delta\Omega$ requires derivation of a large number of scattering acts and the respective numerical code becomes extremely time-consuming. In order to overcome this difficulty we propose a hybrid approach involving ‘very small’ $\Delta\Omega_C$ ($\sim 0.5\gamma^{-1}$) close to the shock, where the scattering details play a role, and much larger scattering amplitude $\Delta\Omega_F = 9^\circ$ to describe particle diffusion further away from the shock. The respective scaling of the scattering time Δt is performed in both cases ($\Delta\Omega_C^2 / \Delta t_C = \Delta\Omega_F^2 / \Delta t_F$) to yield the same turbulence amplitudes measured by the values of the cross-field diffusion coefficient, κ_\perp and the parallel diffusion coefficient κ_\parallel . For a few instances we checked the validity of this approach by reproducing the results for the small $\Delta\Omega_C$ everywhere.

For simplicity, except sections 4.1 and 4.3, we use the same scattering pattern ($\Delta\Omega$ and Δt in units of r_g/c) upstream and downstream the shock, leading to the same values of $\kappa_\perp / \kappa_\parallel$ in these regions (see, however, Ostrowski 1993). One should note that the particle momentum scattering due to the presence of the turbulent

magnetic field is equivalent to the effective magnetic field larger than the respective uniform mean component, B_1 or B_2 . In our model, the effective field can be estimated as

$$B_{e,i} = B_i \sqrt{1 + \left(0.67 \frac{\Delta\Omega}{\Delta t}\right)^2} \quad (i = 1, 2) \quad . \quad (2.15)$$

It is the lower limit for the actual field since the amount of power in perturbations with wave-lengths smaller than $c\Delta t$ cannot be considered within such a simple model. The amount of energy in magnetic turbulence with the waves shorter than $c\Delta t$ is required to be small because the presented estimate assumes the particle momentum perturbation in Δt occurs on the uniform effective perturbing field. To compare the scattering processes with different Δt one has to neglect the unknown factor of the ratio of the averaged actual magnetic field to the estimated value (like the one in Eq. 2.15). Let us note that this factor, as well as the notion of the effective field were not considered earlier.

For relativistic shocks the derived acceleration time scales are presented in units of the formal diffusive scale $T_0 \equiv 4(\kappa_{n,1}/U_1 + \kappa_{n,2}/U_2)/c$ or in units of $r_{e,1}/c$, in the shock normal rest frame but for ultrarelativistic ones in units of $r_{g,2}/c$ in the downstream plasma rest frame.

2.4 Fitting the spectrum and the acceleration time

Our numerical calculations involve particles with momenta systematically increasing over several orders of magnitude. In order to avoid any energy dependent systematic effect we consider the situation with all spatial and time scales – defined by the diffusion coefficient, the mean time between scatterings and the shock velocity – to be proportional to the particle gyroradius, $r_g = p/(eB)$, i.e. to its momentum.

For a chosen shock velocity and the magnetic field configuration we inject particles in the shock at some initial momentum p_0 and follow their phase-space trajectories. We assume the constant particle injection to continue in time after the initial time $t_0 = 0$. A particle is excluded from simulations if it escapes through the free-escape boundary placed far downstream of the shock or reaches the energy larger than the assumed upper limit. These particles are replaced with the ones arising from splitting the remaining high-weight particles, preserving their physical parameters (cf. Kirk & Schneider 1987b; Ostrowski 1991). Particles that exist longer than the time upper limit for simulations are excluded from simulations without replacing. Here we put the boundary at the distance $6\kappa_{2,n}/U_2 + 4r_{g,2}$ for relativistic and $4r_{g,2}$ for ultrarelativistic shocks. We checked by simulations that any further increase of this distance does not influence the results in any noticeable way. For every shock crossing, the particle weight factor multiplied by the inverse of the particle velocity normal to the shock (\equiv particle density) is added to the respective time and momentum bin of the spectrum as measured in the shock normal rest

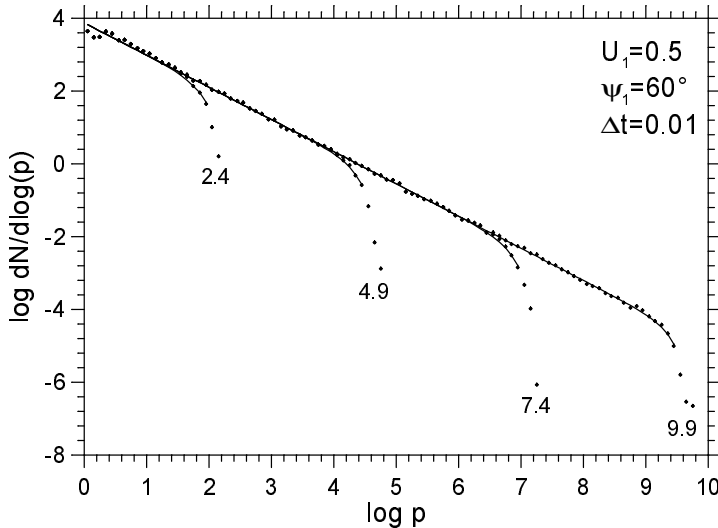


Figure 2.3: Particle spectra at a sequence of time instants. Individual simulation points represent the particle number (weight) ΔN per logarithmic momentum bin $\Delta \log p$. With full lines we present the respective fits (2.16).

frame. As one considers a continuous injection in all instants after t_0 , in order to obtain the particle spectrum at some time $t_j > t_0$ one has to add to particle density in a bin p_i at t_j the densities in this momentum bin for all the earlier times. The resulting particle spectra are represented as power-law functions with the squared exponential cut-off in momentum

$$f(p, t) = A p^{-\alpha} e^{-\left(\frac{p}{p_c}\right)^2} \quad . \quad (2.16)$$

In this formula three parameters are to be fitted: the normalization constant A , the spectral index for the stationary solution α , and the momentum cut-off p_c (Fig. 2.3). Any simulated spectrum evolved in time by increasing the width of its power-law section and thus the best fit of this power-law was possible with the use of the final spectrum at maximum time. Therefore, in the simulations we used the last spectrum to fit parameters A and α . Next, for any earlier spectrum, these parameters were assumed to be constant and we were fitting only the cut-off momentum, p_c . For each fit we used 20 last points of the spectrum preceding the point where particle density fell below 0.16 of $A p^{-\alpha}$. The number of 0.16 was chosen experimentally in order to obtain the best fits to the cut-off region of the spectrum. As the distribution (2.16) represents only an approximation to the actual particle distribution, there was no reason to use points corresponding to lower densities of lesser statistical significance.

In the simulations, due to our proportional momentum scaling of the respective quantities, the derived acceleration time scale (2.4) must be also proportional to p , and thus to $r_g(p)/c$. Therefore, this time scale measured in units of $r_g(p_c)/c$ (or $r_e(p_c)/c$) is momentum independent and can be easily scaled to any momentum. The parameter T_r gives the value of the acceleration time scale in units of $r_{e,1}/c$,

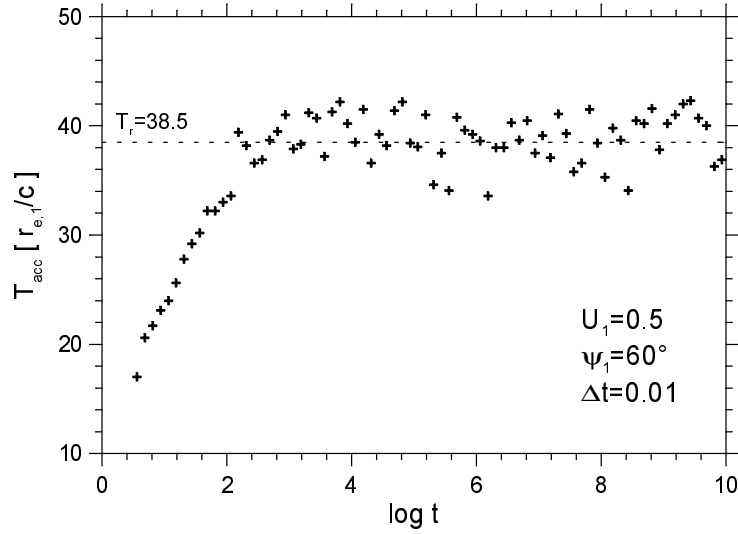


Figure 2.4: An example of simulated values of $T_{acc}^{(c)}$ in units of $r_{e,1}/c$ in a single run of the code. The simulation time t is given in units of $r_{g,1}(p = p_0)/c$ in the shock normal rest frame. We fit the final acceleration time scale only to the points at the advanced phase of acceleration (dashed line). The dispersion of these points defines the fitting error.

i.e. $T_{acc}^{(c)} = T_r r_{e,1}/c$. The value of $T_{acc,i}^{(c)}$ at a particular time t_i is derived from the respective values of $p_{c,i}$:

$$T_{acc,i}^{(c)} = \frac{p_{c,i}}{\frac{p_{c,i} - p_{c,i-1}}{t_i - t_{i-1}}} \quad , \quad (2.17)$$

where we consider the advanced phase of acceleration ($p_{c,i} \gg p_0$). As in our simulations $p_c \propto t$ the condition $(p_{c,i} - p_{c,i-1})/p_{c,i} \ll 1$ is not required to hold in equation (2.17). Therefore, with all scales proportional to the particle momentum, the formula (2.17) reduces to $T_{acc,i}^{(c)} = t_i$ and the parameter T_r tends to a constant (Fig. 2.4). The extension of the simulated spectra over several decades in particle energy allows to avoid problems with the initial conditions and decrease the relative error of the derived time scale by averaging over a larger number of instantaneous $T_{acc,i}$.

Chapter 3

The acceleration time scale in relativistic shock waves

For a given relativistic shock velocity particle anisotropy in the shock depends on the mean magnetic field inclination to the shock normal and the form of turbulent field. Below, we describe the results of simulations performed in order to understand the time dependence of the acceleration process in various conditions. In order to do that we consider shock waves propagating with velocities $U_1 = 0.3, 0.5, 0.7$ and 0.9 of the velocity of light and the magnetic field inclination: $\psi_1 = 1^\circ, 25.8^\circ, 45.6^\circ, 60^\circ, 72.5^\circ, 84.3^\circ$ and 89° . The first one is for a parallel shock, the last two ones are for perpendicular super-luminal shock with all velocities U_1 . The intermediate values define luminal shocks ($U_1/\cos\psi_1 = 1.0$) at the successive velocities considered, respectively $U_1 = 0.9, 0.7, 0.5$ and 0.3 .

In all these cases we investigate the role of varying magnitude of turbulence characterized here by the value of Δt or by the ratio of the diffusion coefficient across the mean field and that along the field, $\kappa_\perp/\kappa_\parallel$. The relation between these parameters for $\Delta\Omega = 10^\circ$ is presented in Fig. 3.1 where at $\Delta t > 0.01$ the presented relation has the power-law form $\kappa_\perp/\kappa_\parallel = 6.3 \cdot 10^{-5} (\Delta t)^2$.

3.1 Parallel shocks

The most simple case for discussion of the first-order Fermi acceleration is a shock wave with parallel configuration of the mean magnetic field. As an example we consider the shock with negligible field inclination $\psi_1 = 1^\circ$. For such a shock, the present simulations confirm the expected relation of decreasing the acceleration time scale with increasing the shock velocity and the amplitude of trajectory perturbations (Fig. 3.2). One should note at the upper panel of the figure that for short Δt the presented time scales decrease more and more slowly with decreasing Δt . It is due to the fact that starting from some value of Δt we reach conditions of nearly isotropic diffusion, $\kappa_\parallel \approx \kappa_\perp$ and further decreasing of the time delay between scatterings decreases the acceleration time in much the same proportion as the time

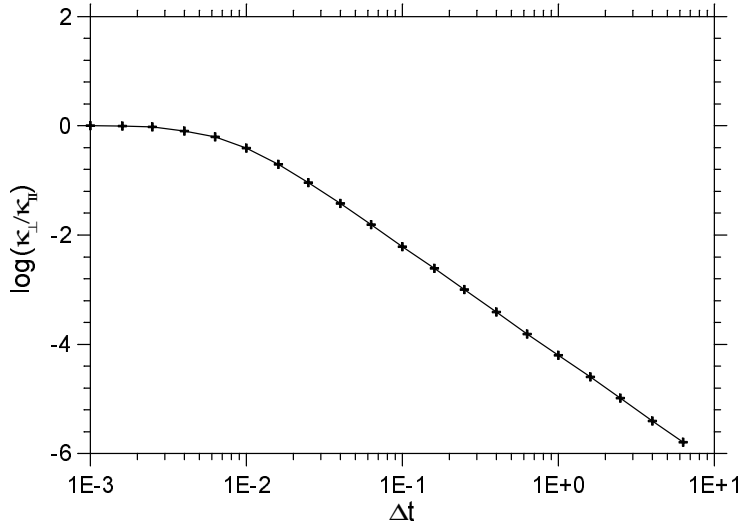


Figure 3.1: The relation between the scattering parameter Δt and the respective ratio of diffusion coefficients $\kappa_\perp/\kappa_\parallel$.

unit $r_{e,1}/c$ used to measure it (cf. Eq. 2.15, Fig. 3.1). In the lower panel of Fig. 3.2 the diffusive time scale T_0 ($\equiv 4(\kappa_{n,1}/U_1 + \kappa_{n,2}/U_2)/c$) is used as the time unit. The minute differences between the successive curves reflect the statistical fluctuations arising during simulations. Without such fluctuations all curves should coincide. The one sigma fit errors of $T_{acc}^{(c)}$ are indicated near the respective points. One should note that for increasing the shock velocity the acceleration time scale decreases with respect to the diffusive time scale.

3.2 Variation of $T_{acc}^{(c)}$ with magnetic field inclination

In order to compare the acceleration time scales for different magnetic field inclinations ψ_1 we performed simulations assuming a constant scattering parameters upstream and downstream yielding the same ratio of $\kappa_\perp/\kappa_\parallel$ in these regions. However, due to shock compression the particle gyration period is shorter downstream than upstream in proportion to the *mean* magnetic field compression (Eq. 2.13). In Fig. 3.3 we present the values of the acceleration time scale derived in such conditions at different ψ_1 . For super-luminal shocks the results are presented for the cases allowing for particle power-law energy spectra, i.e. when the cross-field diffusion is sufficiently effective. Actually, the spectra with inclinations $\alpha < 10.0$ are only included.

In general, the acceleration time scale decreases with increasing field inclination, reaching in some cases the values comparable, or even smaller than the particle upstream gyroperiod (6.28 in our units of $r_{e,1}/c$). The trend can be reversed for intermediate wave amplitudes when the magnetic field configuration changes into the

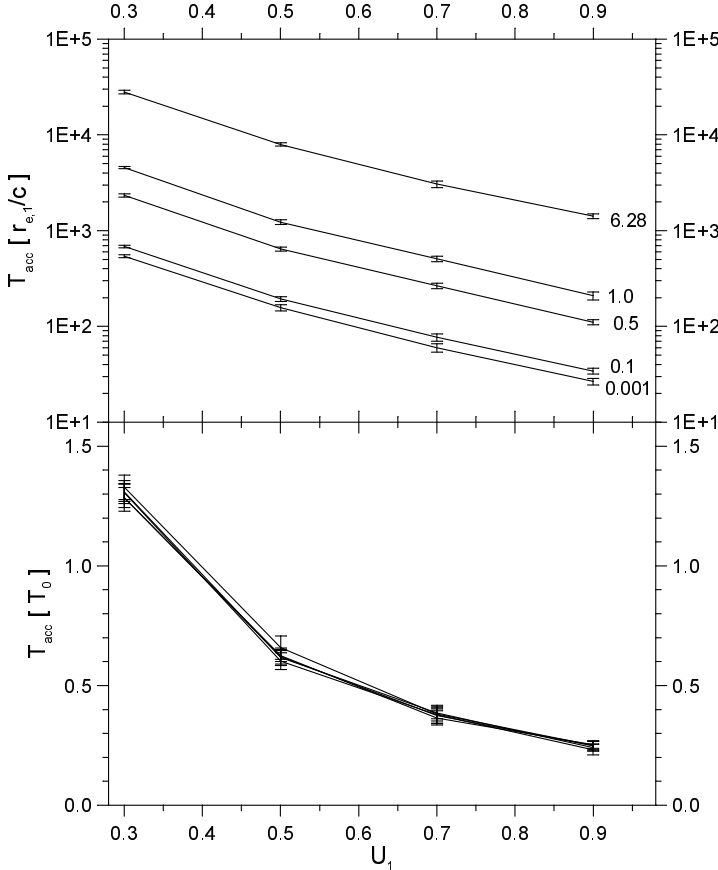


Figure 3.2: The values of $T_{acc}^{(c)}$ in parallel shock waves ($\psi_1 = 1^\circ$) in units of a.) $r_{e,1}/c$ and b.) T_0 versus the shock velocity U_1 . The values resulting from simulations are given for $U_1 = 0.3, 0.5, 0.7$ and 0.9 with the scattering amplitude parameter Δt near the respective results at the upper panel.

luminal and super-luminal one. Such changes are accompanied with the steepening of the spectrum (see below). The acceleration rate at different scattering amplitudes changes with ψ_1 in a way that at different inclinations the minimum acceleration times occur at different perturbation amplitudes (different Δt).

An important feature of the acceleration process in relativistic shocks should be mentioned at this point. The variations of $T_{acc}^{(c)}$ in oblique shocks are accompanied by changes of the particle spectrum inclination (cf. Kirk & Heavens 1989; Ostrowski 1991). In Fig. 3.4, the curves at $(T_{acc}^{(c)}, \alpha)$ plane represent the results for decreasing the scattering amplitude expressed with parameter Δt , and joined with lines for the same magnetic field inclination ψ_1 . For parallel shocks the changes in $T_{acc}^{(c)}$ do not lead to any variation of the spectral index. However, for oblique sub-luminal ($\psi_1 = 25.8^\circ, 45.6^\circ$) and luminal ($\psi_1 = 60^\circ$) shocks a non-monotonic behavior is seen. The trend in changing $T_{acc}^{(c)}$ and α observed at smaller perturbation amplitudes (larger Δt) is reversed at larger amplitudes when the substantial cross-field diffusion is possible.

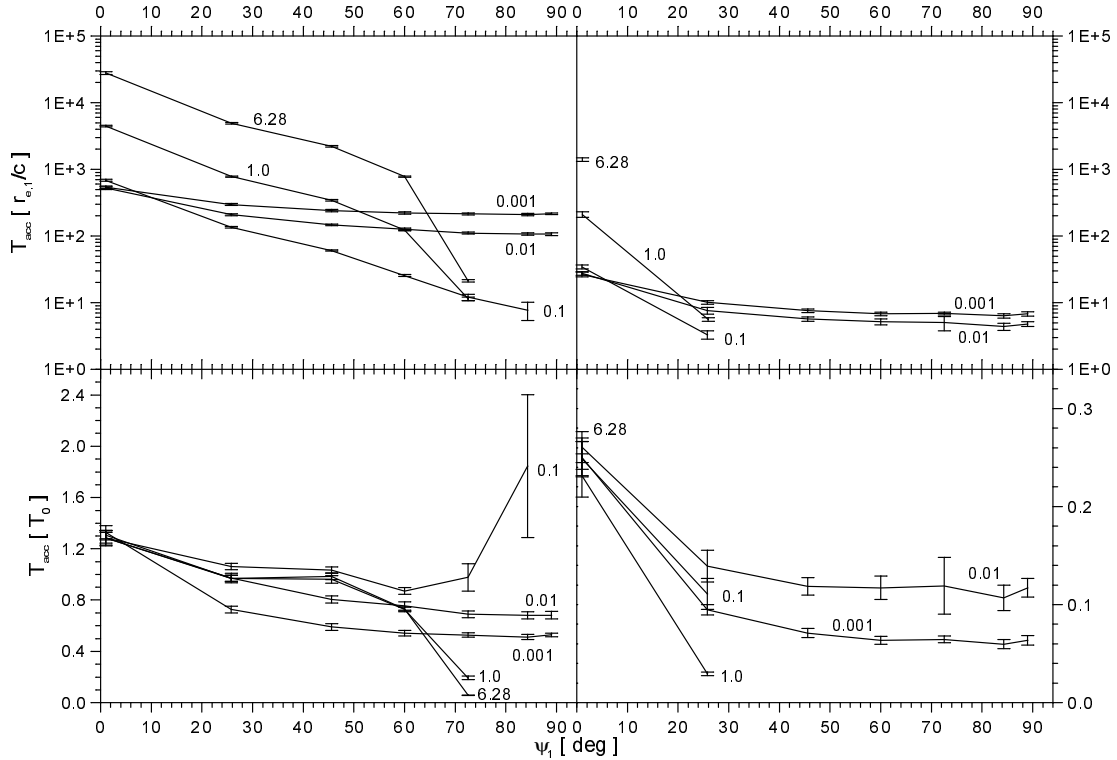


Figure 3.3: The value of $T_{acc}^{(c)}$ in units of $r_{e,1}/c$ (upper panels) and T_0 (lower panels) versus the magnetic field inclination ψ_1 . The values resulting from simulations are presented for $U_1 = 0.3$ (left panels) and 0.9 (right panels) with values of the parameter Δt given near the respective results.

For oblique shocks (cf. Fig. 3.5) we observe an analogous reduction of the acceleration time scale as that reported by Naito & Takahara (1995) with the pitch angle diffusion model allowing for a more rapid acceleration than the large angle scattering model. Of course this agreement is broken for short Δt , where the cross field diffusion can not be neglected and the particle magnetic momentum is not conserved at interactions with the shock.

3.3 Variation of $T_{acc}^{(c)}$ with varying turbulence levels

In a parallel shock the acceleration time scale reduces with the increased turbulence level in its neighborhood. This phenomenon, well known for nonrelativistic shocks (cf. Lagage & Cesarsky 1983), is confirmed here for relativistic shock velocities (Fig. 3.2). In general, there are two main reasons for this change. The first one is a simple reduction of the diffusion time of particles outside the shock due to shorter intervals between scatterings analogous to the decrease observed in nonrelativistic shocks. However, the increased amount of scattering influences also the acceleration

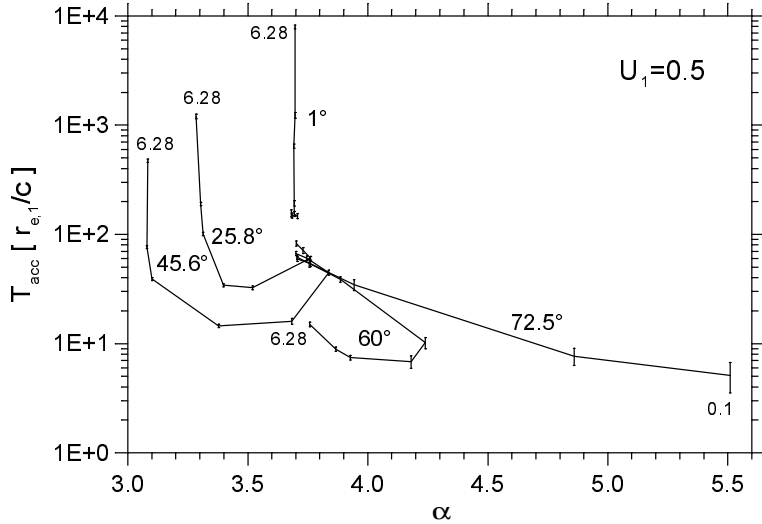


Figure 3.4: The values of $T_{acc}^{(c)}$ in units of $r_{e,1}/c$ at different inclinations ψ_1 versus the particle spectral index α . The values resulting from simulations are given for $U_1 = 0.5$ for five values of the angle ψ_1 given near the respective results. The *maximum* value of Δt is given at the end of each curve and it monotonously decreases along the curve.

process due to changing (decreasing) the particle anisotropy at the shock and thus, modifying the mean energy gain of particles interacting with the shock discontinuity. Additionally, in oblique shocks the upstream-downstream transmission probability may increase. One should note that the present approach is not able to describe fully the effect of decreasing anisotropy with the small amplitude random scattering model applied. It is due to the fact that correlations between the successive modifications of a trajectory (a sequence of small angle scattering acts in this paper) in a single MHD wave cannot be accurately modeled within the simplified approach used. A more exact approach requires integration along the particle trajectories in realistic configurations of the magnetic field. However, the comparison of the present simplified method to the one involving such an integration shows a reasonably good agreement (Ostrowski 1993) suggesting that averaging over realistic trajectories is equivalent in some way to such averaging within our random scattering approach.

In shocks with oblique magnetic fields a non-monotonic change of the acceleration time scale with the amount of scattering along the particle trajectory is observed (Fig. 3.6, see also Fig. 3.3; cf. Ostrowski 1991 for the spectral index). Increasing the amount of turbulence up to some critical amplitude decreases the diffusion time along the magnetic field and thus $T_{acc}^{(c)}$. However, as the mean diffusion time outside the shock is related to the normal diffusion coefficient¹ κ_n ($\kappa_{n,i} = \kappa_{\parallel,i} \cos^2 \psi_i + \kappa_{\perp,i} \sin^2 \psi_i$, $i = 1, 2$), the increasing κ_{\perp} will lead, for large scattering amplitudes to

¹One should note that for the relativistic shocks, due to particle anisotropy, the respective relation may be not so simple as that given in equation (2.2) for nonrelativistic shocks.

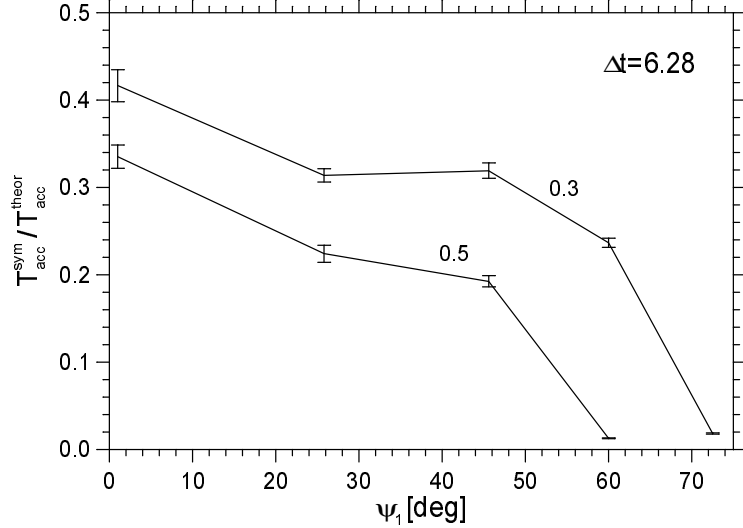


Figure 3.5: The ratio of the pitch angle diffusion simulated time scale T_{acc}^{sym} to the ‘theoretical’ nonrelativistic time scale T_{acc}^{theor} given in Eq. 2.2 for different inclinations of the magnetic field ψ_1 . The results for $U_1 = 0.3$ and 0.5 are presented for the case of negligible cross-field diffusion ($\Delta t = 6.28$ in the pitch angle diffusion model).

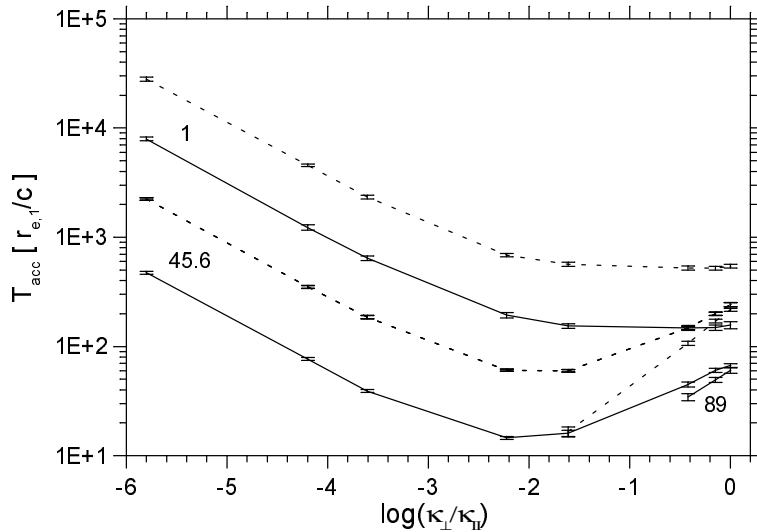


Figure 3.6: The acceleration time $T_{acc}^{(c)}$ versus the level of particle scattering $\kappa_{\perp}/\kappa_{\parallel}$ for shocks with velocity $U_1 = 0.3$ (dashed lines) and 0.5 (full lines). We present results for three values of the magnetic field inclination: a.) parallel shock ($\psi_1 = 1^\circ$), b.) a sub-luminal shock with $\psi_1 = 45.6^\circ$ and c.) a super-luminal shock with $\psi_1 = 89^\circ$.

longer T_{acc} in units of r_e/c . In the units of T_0 the acceleration time depends only weakly on the turbulence level and shows a small maximum for the minimum at the presented figure. For super-luminal shocks one can note the absence of data points corresponding to low turbulence levels, where the power-law spectrum cannot be formed or it is extremely steep. In these excluded cases, the upstream population of energetic particles is only compressed at the shock with the characteristic upstream time of $\sim r_{e,1}/U_1$ (cf. Begelman & Kirk 1990; Ostrowski 1993).

Chapter 4

Ultrarelativistic shock waves

In the present chapter we discussed several aspects of the first order acceleration process active at ultrarelativistic ($\gamma \gg 1$) shock waves. These results are partly published in Bednarz & Ostrowski (1998, 1999) and in Bednarz (1999).

Below the downstream magnetic field is derived for the relativistic shock with the compression R obtained with the formulas of Heavens & Drury (1988) for a cold (e, p) plasma – $R \approx 3.6$ for our smallest value of $\gamma = 3$ and tends to $R = 3$ for $\gamma \gg 1$, as measured in the shock rest frame.

4.1 Acceleration mechanism

A particle crossing the shock to upstream medium has a momentum vector nearly parallel to the shock normal. Then the particle momentum changes its inclination in two ways by: 1) scattering in an inhomogeneous magnetic field and 2) smooth variation in a homogeneous field component. Hereafter, the mean deflection angle in these two cases will be denoted by $\Delta\Omega_S$ and $\Delta\Omega_H$, respectively. The first process is a diffusive one and the second depends on time linearly. That means that with increasing shock velocity, keeping other parameters constant, $\Delta\Omega_S$ decreases slower as a square root of time in comparison with $\Delta\Omega_H$. The Lorentz transformation shows that with $\gamma \gg 1$ even a tiny angular deviation in the upstream plasma rest frame can lead to a large angular deviation in the downstream plasma rest frame. Let us denote a particle phase by φ and the angle between momentum and a magnetic field vector by ϑ both measured in the downstream plasma rest frame. Values of these parameters at the moment when a particle crosses the shock downstream determine if it is able to reach the shock again in the case of neglected magnetic field fluctuations downstream of the shock. In fact a motion in the homogeneous magnetic field carries a particle in such a way that in most cases it cannot reach the shock again. The magnetic field fluctuations perturbing the momentum direction lead to broadening the (φ, ϑ) range that allows particles to reach the shock again. Thus, as we show below for efficient scattering, when $\Delta\Omega_H$ becomes unimportant in comparison to $\Delta\Omega_S$, the spectral index and the acceleration time reach their

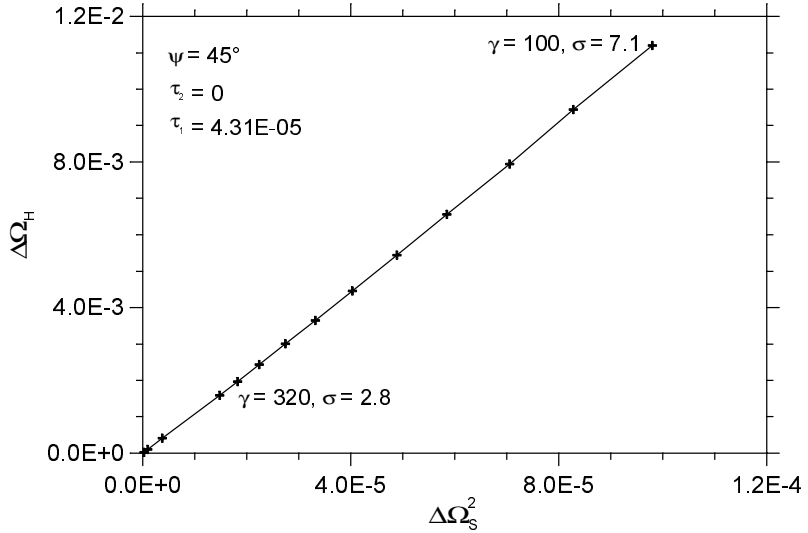


Figure 4.1: The relation between the mean deflection angle upstream of the shock caused by the scattering in an inhomogeneous magnetic field ($\Delta\Omega_S$) and by smooth variation in a homogeneous magnetic field ($\Delta\Omega_H$). Last three points for $\Delta\Omega_H$ below $1 \cdot 10^{-3}$ represent $\gamma = 640, 1280, 2560$ and yield $\sigma = 2.5, 2.3$ and 2.2 respectively.

asymptotic values. The discussed relation between $\Delta\Omega_H$ and $\Delta\Omega_S$ is reproduced in our simulations and presented in Fig. 4.1. There are shown 11 points from $\gamma = 100$ to 320 and three other for $\gamma = 640, 1280, 2560$. The expected linear dependence of these quantities can be noticed.

4.2 Energy spectra

Particle spectral indices were derived for different mean magnetic field configurations, measured by the magnetic field inclination ψ with respect to the shock normal in the upstream plasma rest frame and for different amounts of turbulence measured by $\kappa_\perp/\kappa_\parallel$. In the simulations we considered a few configurations of the upstream magnetic field with inclinations with respect to the shock normal being $\psi = 0^\circ, 10^\circ, 20^\circ, 30^\circ, 60^\circ$ and 90° . The first case represents the parallel shock, the second is for the oblique shock - subluminal at $\gamma = 3$ and a superluminal one at larger γ , and the larger ψ are for superluminal perpendicular shocks for all considered velocities. We applied the same patterns upstream and downstream of the shock for the fluctuation levels $\lambda = -5.34, -4.39, -3.44, -2.49, -1.56, -0.67, -0.16, 0.00$ ($\lambda \equiv \log_{10} \kappa_\perp/\kappa_\parallel$).

In successive panels in Fig. 4.2 the energy spectral indices, σ , for varying ψ and $\kappa_\perp/\kappa_\parallel$ are presented. For a parallel shock ($\psi = 0^\circ$) the amount of scattering does not influence the spectral index and for the growing γ it approaches $\sigma_\infty \simeq 2.2$. One may note that essentially the same limiting value was anticipated for the large- γ parallel shocks by Heavens & Drury (1988). Let us remember that the results for $\psi = 10^\circ$ are for superluminal shocks if $\gamma > 5.75$. In this case, when we go from the

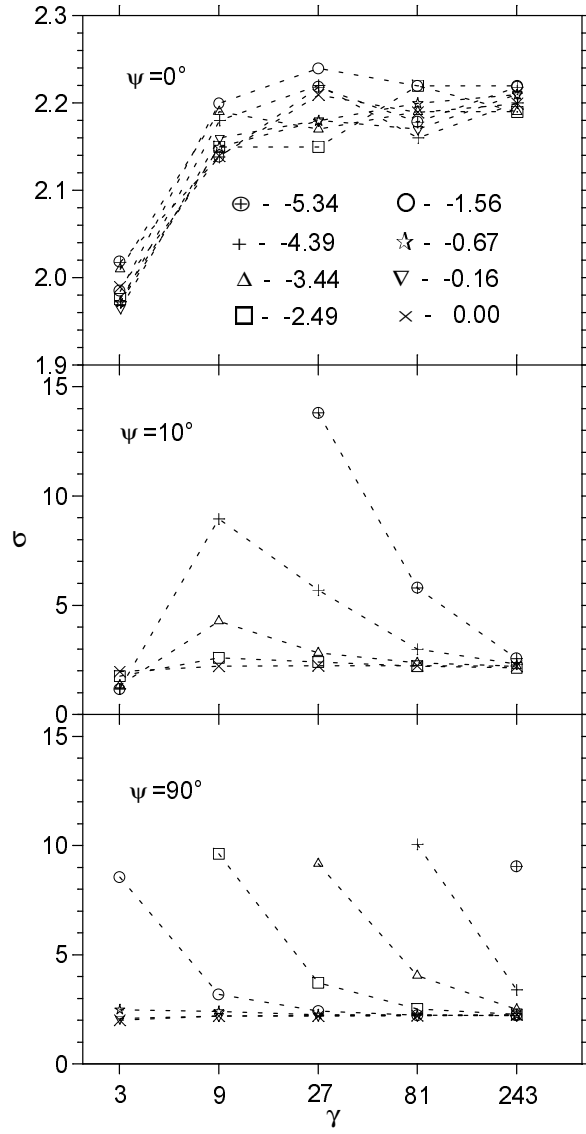


Figure 4.2: The simulated spectral indices σ for particles accelerated at shocks with different Lorentz factors γ . Results for a given $\kappa_{\perp}/\kappa_{\parallel}$ are joined with lines; the respective value of $\log_{10} \kappa_{\perp}/\kappa_{\parallel}$ is marked by the point shape (see upper panel). The results for different magnetic field inclinations ψ are given in the successive panels: (a) $\psi = 0^\circ$, (b) $\psi = 10^\circ$, and (c) $\psi = 90^\circ$.

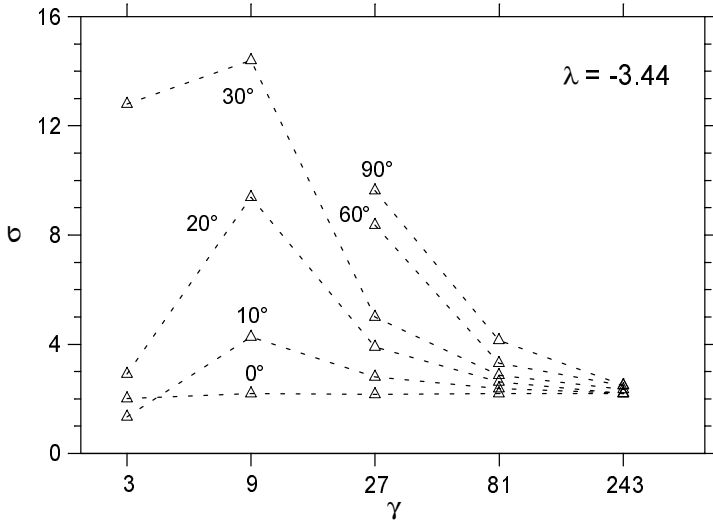


Figure 4.3: The simulated spectral indices σ for particles accelerated at shocks with different Lorentz factors γ . Results for a given upstream magnetic field inclination ψ are joined with dashed lines; the respective value of ψ is given near each curve. The value $\lambda \equiv \log_{10}(\kappa_{\perp}/\kappa_{\parallel})$ is given in the figure.

‘slow’ $\gamma = 3$ shocks to higher γ ones, at first the spectrum inclination increases (σ grows) but at large γ the spectrum flattens to approach the asymptotic value close to 2.2. The spectrum steepening phase is more pronounced for small amplitude perturbations (small $\kappa_{\perp}/\kappa_{\parallel}$), but even at very low turbulence levels the final range of the spectrum flattening is observed. For larger ψ the situation does not change considerably, but the phase of spectrum steepening is wider involving larger values of σ and starting at smaller velocities below the lower limit of our considerations (there may be no such range involving the steepening phase if the required velocity is below the sound velocity).

The spectral indices for different magnetic field inclinations, but for the same value of $\log_{10}(\kappa_{\perp}/\kappa_{\parallel}) = -3.44$ are presented at Fig. 4.3. The large spectral indices occurring in the steepening phase are usually interpreted as a spectrum cutoff. In this case the main factor increasing the particle energy density is a nonadiabatic compression in the shock (Begelman & Kirk 1990).

The particle angular distributions $F(\mu)$ in the $\gamma \gg 1$ shocks can be extremely anisotropic when considered in the upstream plasma rest frame. However, when presented in the shock rest frame the distribution is always ‘mildly’ anisotropic. This feature is illustrated in Fig. 4.4 when γ equals 3 or 27 (note that in Figs. 4.4 - 4.7 the area below each curve is normalized to 100). In the simulations we observed an interesting phenomenon accompanying previously discussed spectrum convergence to the limiting inclination: spectra close to the limit exhibit similar angular distributions at the shock *as measured in the shock rest frame* (Fig. 4.5).

Again, this feature is independent of the background conditions, and the difference between the actual angular distribution and the limiting one reflects the

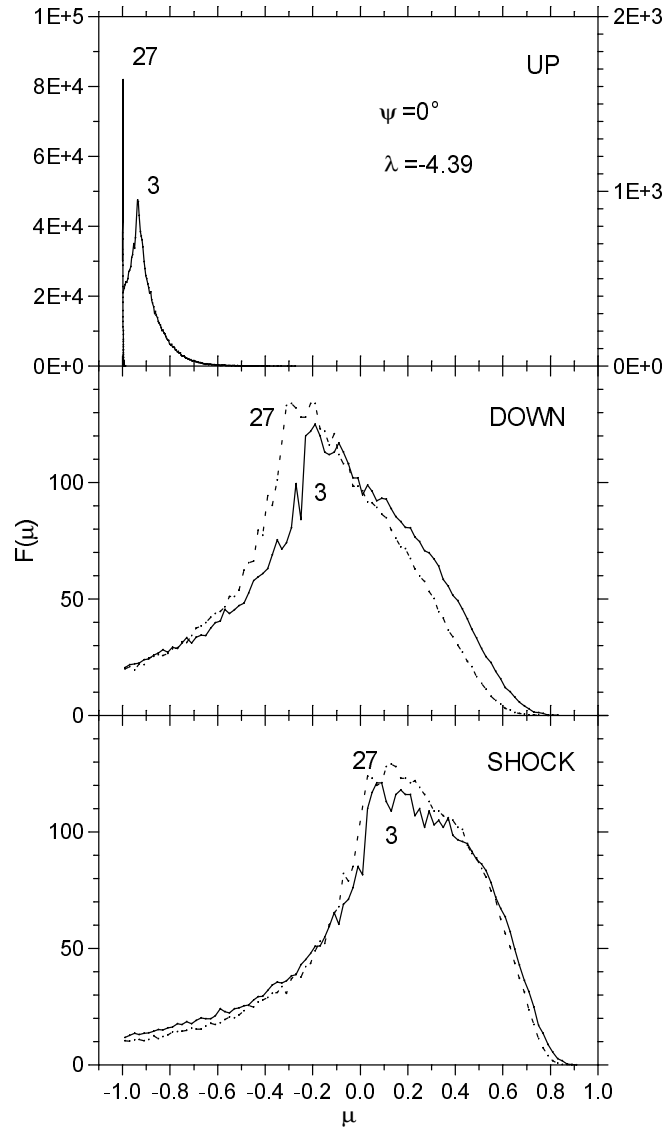


Figure 4.4: The simulated particle angular distributions in the shock in different coordinate frames: UP – the upstream plasma rest frame, DOWN – the downstream plasma rest frame and SHOCK – the shock rest frame. The results are presented for parallel shocks with the Lorentz factors 27 and 3 given near the respective curves. In the upper panel the left axis is for $\gamma = 27$ and the right one for $\gamma = 3$.

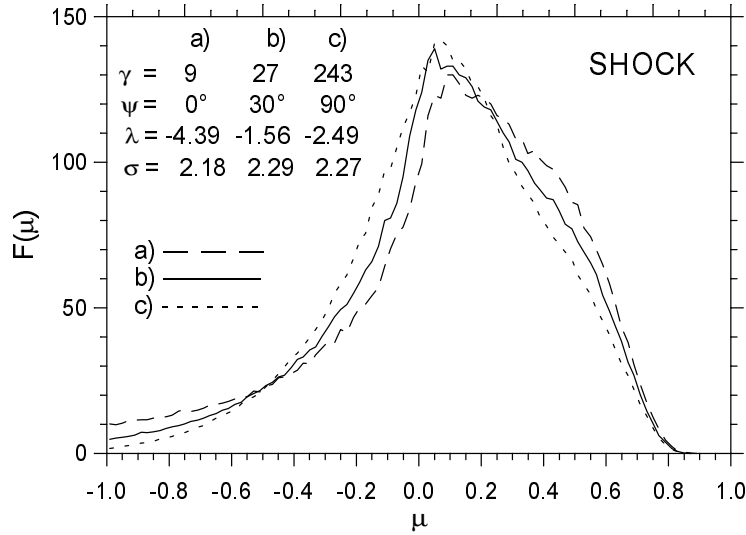


Figure 4.5: Examples of the shock rest frame particle angular distributions for different cases with σ close to σ_∞ .

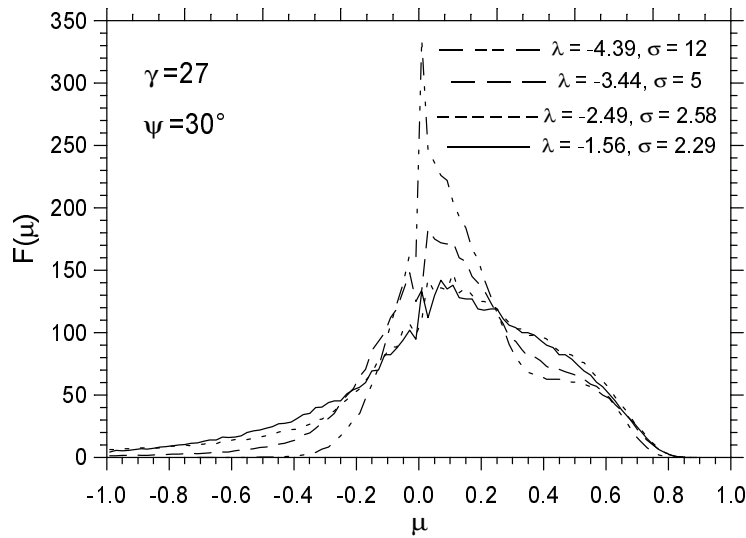


Figure 4.6: The shock rest frame particle angular distributions for $\gamma = 27$ and $\psi = 30^\circ$. Curves are presented for increasing $\lambda \equiv \log_{10} \kappa_\perp / \kappa_\parallel$ and σ approaching σ_∞ . The last curve is the same as the curve (b) at Fig. 4.5

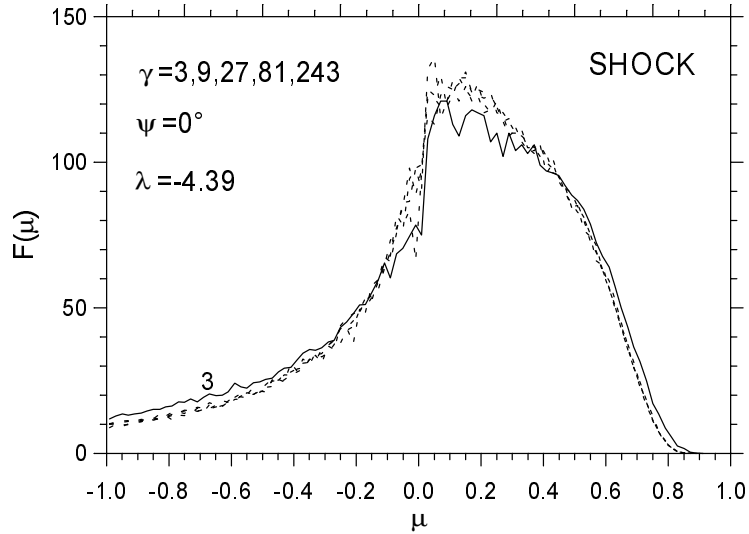


Figure 4.7: The shock rest frame particle angular distributions for parallel shocks with $\gamma = 3, 9, 27, 81, 243$. A visible deviation of the distribution for $\gamma = 3$ (full line) results from the slightly larger compression occurring in such a shock.

difference between the spectral index σ and σ_∞ (cf. Fig. 4.6). For parallel shocks with $\gamma \geq 9$ where the spectral index is essentially constant $\sigma = \sigma_\infty$ this distribution is independent of the value of γ and the perturbation amplitude $\kappa_\perp/\kappa_\parallel$ (Fig. 4.7).

For large γ shocks we observe the convergence of the derived energy spectral indices to the value $\sigma_\infty \approx 2.2$ independent of the background conditions. This unexpected result provides a strong constraint for the acceleration process in large γ shocks and it can be quantitatively explained with arguments presented at the beginning of this chapter. Our interesting finding do not fully explained with such simple arguments is of the belief that the resulting spectral index is the same for oblique and parallel shocks. Our derivations are limited to the test particle approach. However, as the obtained spectra are characterized with $\sigma > 2.0$ any nonlinear back reaction effects are not expected to affect the acceleration process within the spectrum high energy tail with $\sigma \approx \sigma_\infty$.

4.3 The acceleration time scale

In the following simulations we consider shocks with $\gamma = 20, 40, 80, 160, 320$, magnetic field inclinations $\psi = 15^\circ, 30^\circ, 45^\circ, 60^\circ, 75^\circ, 90^\circ$ and downstream values of magnetic field fluctuations $\tau_2 = 0, 1.0 \cdot 10^{-3}, 1.1 \cdot 10^{-2}, 0.11, 0.69$.

Simulations prove that fluctuations upstream of the shock (measured by τ_1 , $\tau \equiv \kappa_\perp/\kappa_\parallel$) and downstream of the shock (measured by τ_2) influence the acceleration process independently. The minimum fluctuations upstream of the shock needed to run the acceleration process efficiently tend to zero when $\gamma \rightarrow \infty$. We checked by simulations with different τ_2 that its value does not influence the spectral index

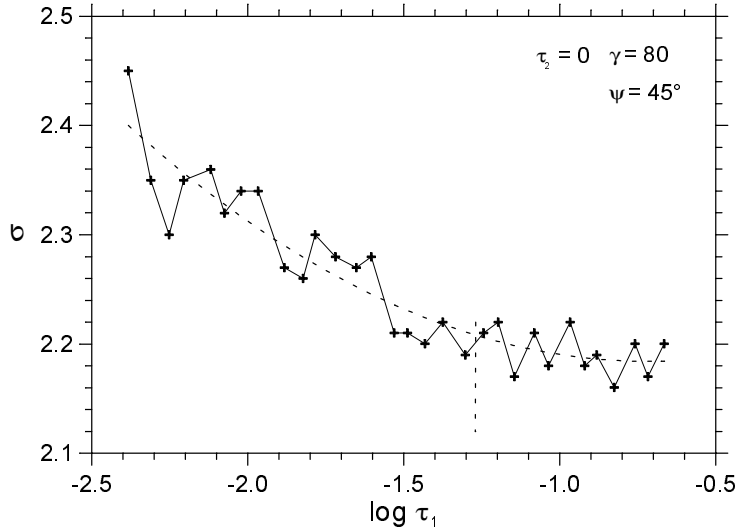


Figure 4.8: Simulated spectral indices as a function of magnetic field fluctuations upstream of the shock. Fluctuations downstream of the shock are neglected. The chosen τ_1 value for $\gamma = 80$ and $\psi = 45^\circ$ is pointed by a dashed line. A second-degree polynomial fit is also marked by a dashed line.

considerably for any given τ_1 with exception of only the injection phase of the upstream isotropic distribution.

Thus, as a first case we consider downstream conditions without magnetic field fluctuations. By simple data inspection (cf. Fig. 4.8) we look for minimum τ_1 where the spectral index reaches its limit of 2.2 and we apply this value in further simulations. The relation between τ_1 , γ and ψ can be roughly fitted with the equation $\tau_1 = 0.25 \gamma^{-1.2} \psi$ in the considered range of shock parameters. We repeated simulations for a number of cases with different γ and ψ and $\tau_2 \neq 0$. The obtained results are in good agreement with the ones derived from the above equation up to $\tau_2 = 0.11$.

Values of the acceleration time t_{acc} for three amplitudes of magnetic field fluctuations downstream of the shock are presented in Fig. 4.9. In the figure one can see the lack of change of t_{acc} with ψ but it slowly decreases to the asymptotic value with γ . In the simulations we have observed the tendency of t_{acc} to grow when σ increases up to 2.3-2.4 and no further change if magnetic field fluctuations upstream of the shock grow. For $\tau_2 \leq 0.11$ the asymptotic value of the acceleration time is close to r_g/c . It occurs that r_g/c is a good unit provided that the homogeneous magnetic field dominates the randomly component. Unfortunately, when this condition fails the meaning of t_{acc} becomes unclear in the simulations then. For this reason we will not discuss further the case of $\tau_2=0.69$.

Approximate calculations of Gallant & Achterberg (1999) showed that $t_U^U/t_U^D \simeq 1$, where t_U^U is the particle mean residence time upstream of the shock (upper index) as measured in the upstream plasma rest frame (lower index), and D in t_U^D stands for the downstream residence time. However, they were not able to consider the

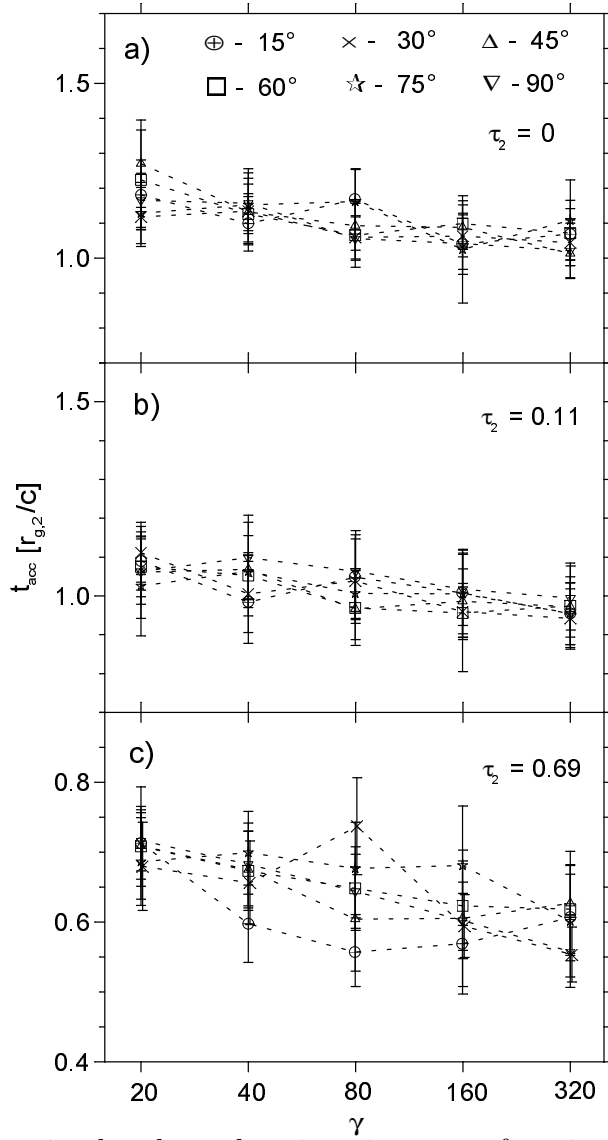


Figure 4.9: The simulated acceleration time as a function of the shock Lorentz factor: a) without fluctuations downstream of the shock, b) with fluctuations downstream of the shock, c) fluctuations downstream of the shock dominate homogeneous magnetic field. Results for a given upstream magnetic field inclinations given in panel a) are joined with dashed lines.

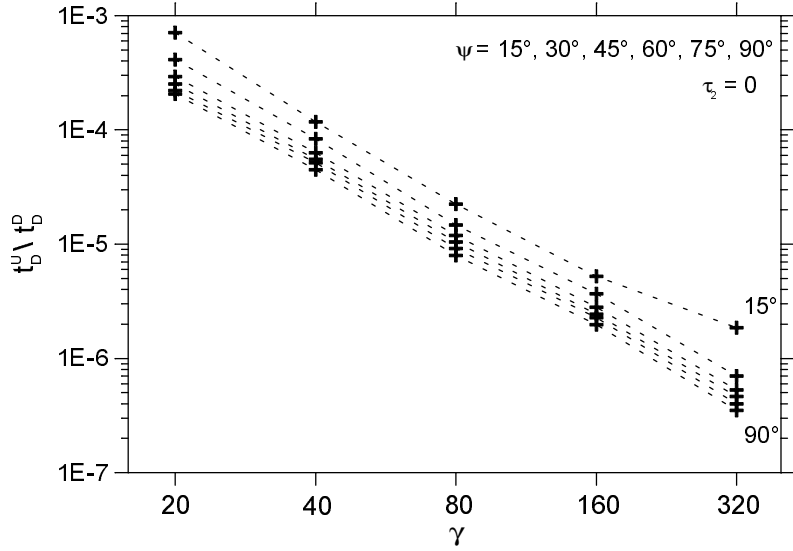


Figure 4.10: The ratio of the mean time a particle spends upstream of the shock to the time it spends downstream of the shock as a function of the shock Lorentz factor. It slightly decreases with growing upstream magnetic field inclination. Dashed lines join points with a constant ψ . Apparent deviation of the point with $\gamma = 320$, $\psi = 15^\circ$ is real.

anisotropic particle momentum distribution and our results in Fig. 4.10 *transformed to the upstream plasma rest frame* with t_U^U/t_U^D within the range $0.01 - 0.1$ are more adequate for real situations. Additionally, the above authors applied an extremely irregular magnetic field upstream of the shock represented by randomly oriented magnetic cells with field amplitude B and they measured time in the upstream unit of $r_g(B)/c$. As a result they obtained that t_U^U/t_U^D could be much larger than 1 in the case.

Just before the spectral index reaches its minimal value (cf. Fig. 4.8) $\Delta\Omega_S$ stabilizes near the limit which value does not further depend on the magnetic field inclination as is seen in Fig. 4.11. Momentum vectors of particles crossing downstream of the shock have similar distributions as measured in the downstream plasma rest frame if $\Delta\Omega_S$ approaches the maximum value. Then, it follows that parameters we consider below depend only on τ_2 .

For growing τ_2 ($\tau_2 = 0, 1.0 \cdot 10^{-3}, 1.1 \cdot 10^{-2}, 0.11$) ¹ the acceleration time is constant and accompanied by a slow increase of the mean energy gain in one cycle downstream-upstream-downstream $\langle \Delta E/E \rangle_D = 0.89, 0.94, 1.0, 1.1$, and a slight decrease of the fraction of particles that reach the shock again after crossing it downstream, $\langle \Delta n/n \rangle = 0.51, 0.50, 0.48, 0.44$. Simultaneously the mean time a particle spends downstream of the shock grows as $t_D^D = 0.96, 1.0, 1.2, 1.35$. Time that a particle spends upstream of the shock can be neglected in this rest frame as is visible

¹Below, we provide the respective series of a given simulated parameter for this sequence of τ_2 .

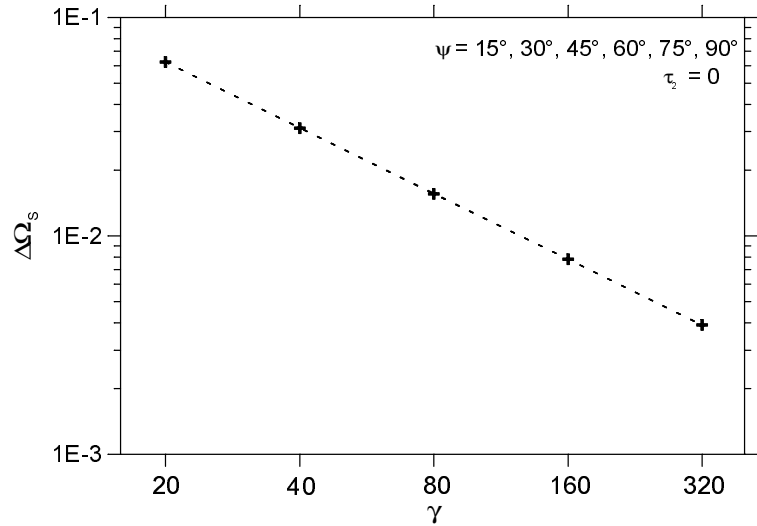


Figure 4.11: The mean deflection angle resulting from scattering in an inhomogeneous magnetic field upstream of the shock as a function of the shock Lorentz factor γ with τ_1 chosen in a way as illustrated in Fig. 4.8. Six dashed lines for different ψ are identical.

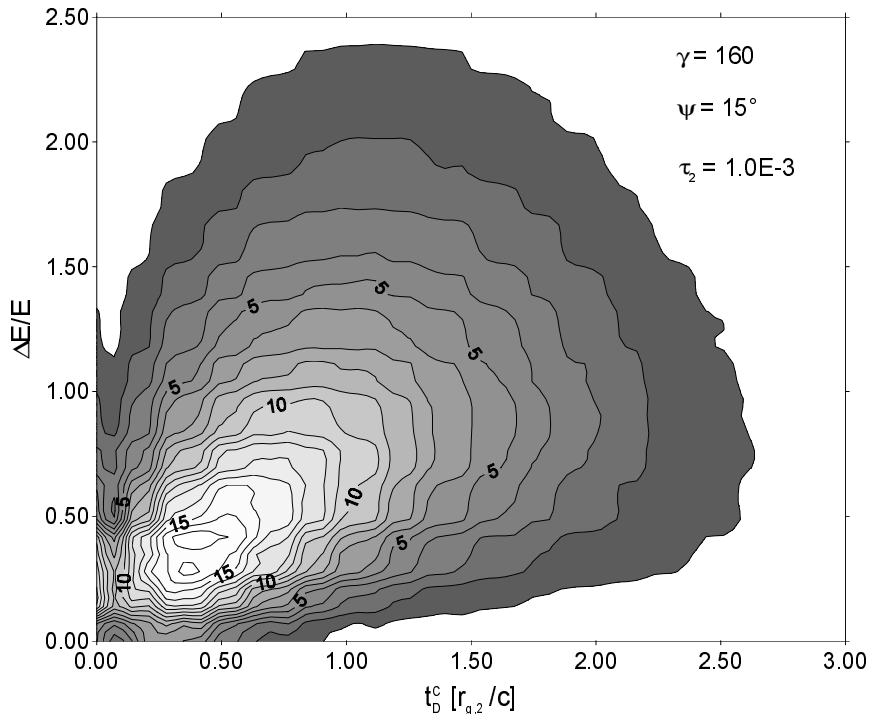


Figure 4.12: Distribution of particle energy gains $\Delta E/E$ as measured in the downstream plasma rest frame during one cycle ‘C’ downstream-upstream-downstream versus the time $t_D^C[r_{g,2}/c]$. The shock parameters are given in the picture. The mean energy gain $\langle \Delta E/E \rangle_D$ grows with t_D^C up to $t_D^C \simeq 2$ and decreases afterwards.

in Fig. 4.10. It implies, approximately,

$$t_{acc} = t_D^D / \langle \Delta E / E \rangle_D \quad (4.1)$$

if one neglects correlations between these quantities (cf. Fig. 4.12). Similarly we can roughly estimate the value of the energy spectral index of accelerated particles as

$$\sigma \simeq 1 - \ln(\langle \Delta n / n \rangle) / \ln(\langle \Delta E / E \rangle_D + 1) \quad . \quad (4.2)$$

4.4 The acceleration through particle reflection

Particles with an initial momentum p_0 taken as the momentum unit, $p_0 = 1$, were injected at the distance of $2r_g$ (r_g - particle gyroradius) upstream of the shock front. For all particles we derived their trajectories until crossing the shock downstream, and then upstream, or were advected with the downstream plasma, to reach a distance of $4r_g$ downstream of the shock. For each single particle interaction with the shock the particle momentum vector was recorded so we were able to consider angular and energy distributions of such particles. We considered shocks with Lorentz factors $\gamma = 10, 160$ and 320 . For each shock we discussed the acceleration processes in conditions with the magnetic field inclinations $\psi = 0^\circ, 10^\circ, 70^\circ$ and with 16 values for the turbulence amplitude measured by the ratio τ of the cross-field diffusion coefficient κ_\perp to the parallel diffusion coefficient κ_\parallel . The applied values of τ were taken from the range of $(3.2 \cdot 10^{-6}, 0.95)$, approximately uniformly distributed in $\log \tau$. In each simulation run we derived trajectories of $5 \cdot 10^4$ particles with the initial momenta isotropically distributed in the upstream rest frame.

In the downstream plasma rest frame the shock moves with velocity $c/3$. This velocity is comparable to the particle velocity c . Therefore, from all particles crossing the shock downstream only the ones with particular momentum orientations will interact with the shock again; the remaining particles will be caught in the downstream plasma flow and advected far from the shock front. In the simulations we considered this process quantitatively. However, let us first present a simple illustration.

Large compression ratios occurring in ultrarelativistic shocks, as measured between the upstream and downstream plasma rest frames, lead for nearly all oblique upstream magnetic field configurations to the quasi-perpendicular configurations downstream of the shock. Thus, let us consider for this illustrative example a shock with a non-perturbed perpendicular downstream magnetic field distribution. Particle crossing the shock downstream with inclination to the magnetic field ϑ and the phase φ – both measured in the downstream plasma rest frame, $\varphi = \pi/2$ for a particle velocity normal to the shock and directed downstream – will be able to cross the shock upstream only if the equation

$$\frac{c}{3} t = r_g [\cos(\varphi + \omega_g t) - \cos \varphi] \quad (4.3)$$

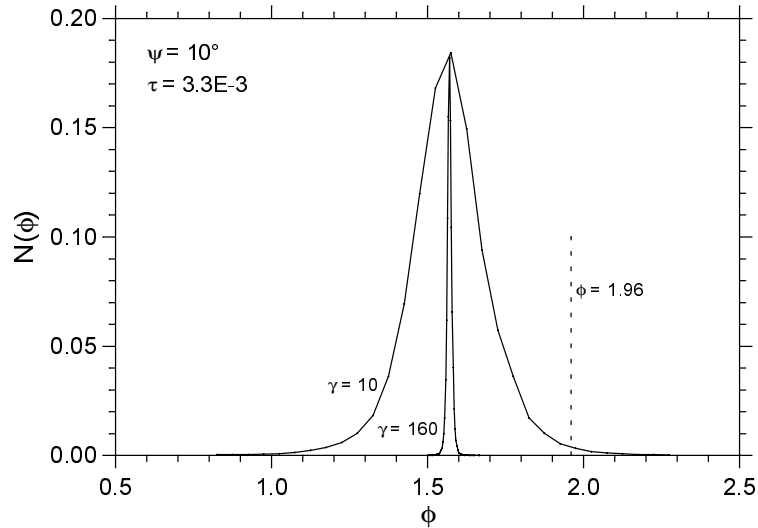


Figure 4.13: A distribution of particle phases for particles crossing the shock downstream (as measured in the downstream plasma rest frame), if their upstream distribution was isotropic. A dashed line delimits a range of particle phases below which particles are not able to reach the shock again at the perpendicular uniform downstream magnetic field.

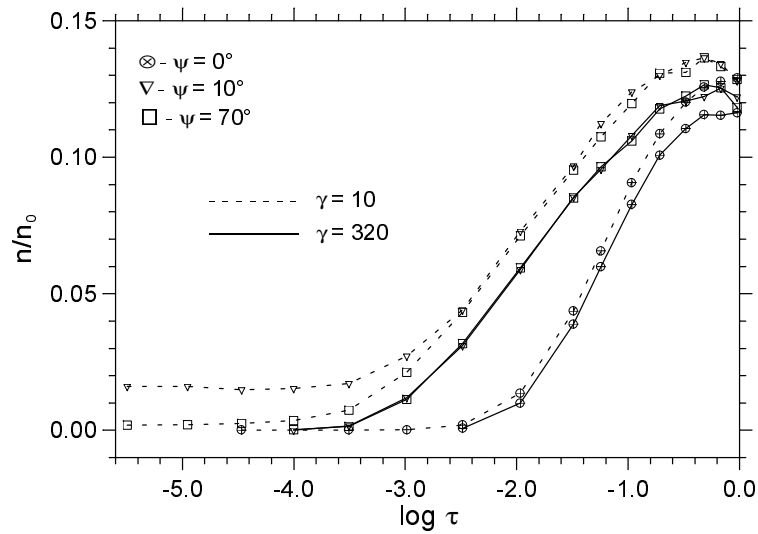


Figure 4.14: A ratio of the number of reflected particles, n , to all particles crossing the shock downstream, n_0 , as a function of the magnetic field fluctuations amplitude, τ .

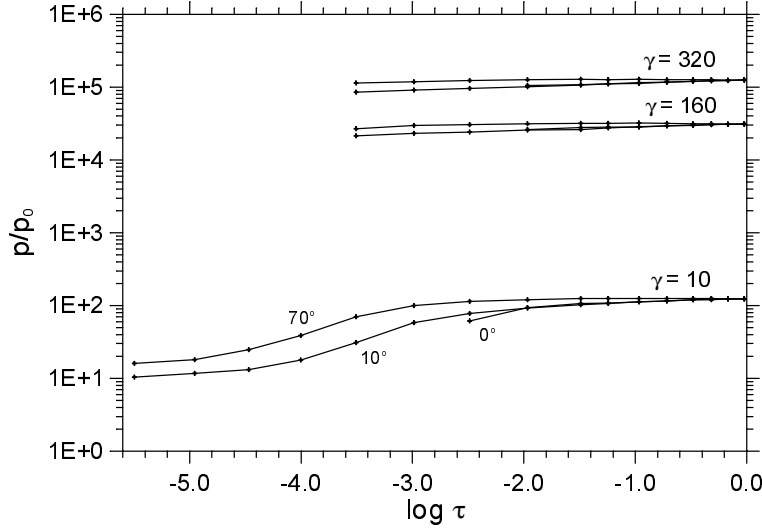


Figure 4.15: Momentum gains of reflected particles, p/p_0 , as a function of the magnetic field fluctuations amplitude τ . For large magnetic field fluctuations the momentum gain approaches $\approx 1.2\gamma^2$ independently of the shock Lorentz factor.

has a solution at positive time t . Here $r_g = \frac{pc}{eB} \sin \vartheta$ is the particle gyroradius, $\omega_g = \frac{eB}{p}$ is the gyration frequency, and other symbols have the usual meaning.

An angular range in the space (ϑ, φ) enabling particles crossing the shock downstream to reach the shock again can be characterized for illustration by three values of ϑ . Particles with $\sin \vartheta = 1$ are able to reach the shock again if $\varphi \in (1.96, 3.48)$, with $\sin \vartheta = 0.5$ if $\varphi \in (2.96, 3.87)$ and with $\sin \vartheta = 1/3$ only for $\varphi = 4.71$. That means that all particles with φ smaller than 1.96 (Fig. 4.13) are not able to reach the shock again if fluctuations of the magnetic field downstream of the shock are not present.

For perturbed magnetic fields some downstream trajectories starting in the (ϑ, φ) plane outside the reflection range can be scattered toward the shock to cross it upstream. We prove it by simulations presented in Fig. 4.14. One may observe that increasing the perturbation amplitude leads to an increased number of reflected particles reaching $\approx 13\%$ in the limit of $\tau = 1$. For large magnetic field fluctuations the mean relative energy gains of reflected particles are close to $1.2\gamma^2$ for the shock Lorentz factors considered. One may note a variation of the energy gain with growing τ . The points resulting from simulations for the smallest values of τ were not included in Fig. 4.15 because of the small number of reflected particles (cf. Fig. 4.14).

Chapter 5

Summary

We performed Monte Carlo simulations for shock waves with parallel and oblique (either, sub-luminal and super-luminal) magnetic field configurations with different amounts of scattering along particle trajectories. Field perturbations with amplitudes ranging from very small ones up to $\delta B \sim B$ are considered.

In chapter 2 (cf. Bednarz & Ostrowski 1996) we demonstrate the existence of correlation between particle energy gains and its diffusive times. The analogous correlation is expected for the probability of particle escape downstream the shock. Therefore, for defining the acceleration time scale we use the rate of change of the spectrum cut-off momentum which accommodate all such correlations.

Acceleration times scales in relativistic shocks are discussed in chapter 3 (cf. Bednarz & Ostrowski 1996). In parallel shocks $T_{acc}^{(c)}$ diminishes with the growing perturbation amplitude and the shock velocity. However, it is approximately constant for the increasing turbulence level if we use the respective diffusive time scale as the time unit. Another feature discovered in oblique shocks is that due to the cross-field diffusion $T_{acc}^{(c)}$ can change with δB in a non-monotonic way. The acceleration process leading to the power-law particle spectrum in a super-luminal shock is possible only in the presence of large amplitude turbulence. Then, the shorter acceleration times occur when the perturbations' amplitudes are smaller and the respective spectra steeper. We discussed the coupling between the acceleration time scale and the particle spectral index in oblique shock waves with various field inclinations and revealed a possibility for non-monotonic relations of these quantities. The shortest acceleration time scales seen in the simulations are below the particle gyroperiod upstream of the shock. These times do not require the ultrarelativistic shock velocities, but may occur in mildly relativistic ones with the quasi-perpendicular magnetic field configuration. One should note that due to the larger magnetic field downstream of the shock in this short time the particle trajectory can follow a few revolutions near the shock with only a short section of each one penetrating the upstream region.

The presented estimates of the acceleration time scale provide an interesting possibility for modeling shock waves in the conditions where the electron spectrum cut-off energy is determined by the balance of gains and losses. If one is able to derive

the respective acceleration rate from the knowledge of the energy loss process and the particle spectral index is also known then both these values provide constraints for the acceleration process which could be further used to reduce the parameter space available for the considered shock wave (cf. Fig. 3.4).

In chapter 4 (cf. Bednarz & Ostrowski 1998, 1999; Bednarz 1999) we discussed the acceleration mechanism that holds in ultrarelativistic shocks. We discovered convergence of spectral indices to the universal asymptotic value $\sigma_\infty \simeq 2.2$ and we considered high particle anisotropy that accompanies particle acceleration. The simulations yielded that acceleration time derived from formula applied in ultrarelativistic shocks approximately equals the time derived from the formula neglecting correlations (4.1) and the constant value of 1.0 can be used for $\tau \leq 0.11$.

The presented results are to be applied in models of GRB sources involving ultrarelativistic shock waves (cf. Bednarz 1999). One should note that the mean downstream plasma proton energies can reach there several tens of GeV (cf. Paczyński & Xu 1994) and the lower limit of the considered cosmic ray energies has to be larger than this scale. For shocks propagating in (e^-, e^+) plasma the involved thermal energies are lower, $\sim \gamma$ MeV. These estimates provide the respective lower limits for the accelerated cosmic ray particles. For the physical conditions considered in GRB sources the acceleration process can provide particles with much larger energies limited only by the condition that the energy loss processes (radiative, or due to escape) are ineffective in the downstream gyroperiod time scale. We note a striking coincidence of our limiting spectral index with the value derived for energetic electrons from gamma-burst afterglow observations. Waxman (1997) used a fireball model of GRBs and showed from the functional dependence of the flux on time and frequency that $\sigma = 2.3 \pm 0.1$ in the afterglow of GRB 970228. Galama et al. (1998) made two independent measurements of the electron spectrum index in the afterglow of GRB 970508 which was very close to 2.2.

In the end we have shown that efficiency of ' γ^2 ' reflections in ultrarelativistic shock waves strongly depends on fluctuations of magnetic field downstream of the shock. In the most favorable conditions with high amplitude turbulence downstream the shock the reflection efficiency is a factor of 10 or more smaller than the values assumed by other authors. Moreover, due to the magnetic field compression at the shock we do not expect the required large values of $\kappa_\perp/\kappa_\parallel$ to occur behind the shock (cf. a different approach of Medvedev & Loeb 1999). Therefore, with the actual efficiency of 1 - 10 % there is an additional difficulty for models postulating UHE particle acceleration at GRB shocks (cf. Gallant & Achterberg 1999). Let us note, however, that the mean downstream trajectory of the reflected particle involves only a fraction of its gyroperiod. Thus the presence of compressive long waves in this region leading to non-random trajectory perturbations could modify our estimates.

Chapter 6

Bibliography

Appl, S., Camenzind, M., 1988, Astron. Astrophys. **206**, 258

Axford W. I., Leer E., Skadron G., 1977, in Proc. 15th Int. Cosmic Ray Conf. **11**, p. 132, Plovdiv

Ballard K. R., Heavens A. F., 1991, Mon. Not. R. Astron. Soc. **251**, 438

Ballard K. R., Heavens A. F., 1992, Mon. Not. R. Astron. Soc. **259**, 89

Bednarz J., 1998, in Proc. 16th European Cosmic Ray Symposium, p. 287, Alcalá de Henares

Bednarz J., 1999, submitted

Bednarz J., Ostrowski M., 1996, Mon. Not. R. Astron. Soc. **283**, 447

Bednarz J., Ostrowski M., 1997a, in Proc. Conf. Relativistic Jets in AGN's, p. 158, Cracow

Bednarz J., Ostrowski M., 1997b, in Proc. 25th Int. Cosmic Ray Conf. **4**, p. 385, Durban

Bednarz J., Ostrowski M., 1998, Phys. Rev. Lett. **80**, 3911

Bednarz J., Ostrowski M., 1999, Mon. Not. R. Astron. Soc. **310**, L11

Begelman M. C., Kirk J. G., 1990, Astrophys. J. **353**, 66

Bell A. R., 1978a, Mon. Not. R. Astron. Soc. **182**, 147

Bell A. R., 1978b, Mon. Not. R. Astron. Soc. **182**, 443

Blandford R. D., Königl A., 1979, Astrophys. J. **232**, 34

Blandford R. D., Ostriker J. P., 1978, Astrophys. J. **221**, L29

Decker R. B., 1988, Space Sci. Rev. **48**, 195

de Jager O. C., Harding A. K., Michelson P. F., Nel H. J., Nolan P. L., Sreekumar P., Thompson D. J., 1996, Astrophys. J. **457**, 253

de Hoffman F., Teller E., 1950, Phys. Rev. **80**, 692

Dermer C. D., 1992, Phys. Rev. Lett. **68**, 1799

Chandrasekhar S., 1943, Rev. Mod. Phys. **15**, 1

Chiueh T., Li Z., Begelman M. C., 1998, Astrophys. J. **505**, 835

Ellison D. C., Jones F. C., Reynolds S. P., 1990, Astrophys. J. **360**, 702

Fermi E., 1949, Phys. Rev. **75**, 1169

Galama T. J., Wijers R. A. M. J., Bremer M., Groot P. J., Strom R. G., de Bruyn

A. G., Kouveliotou C., Robinson C. R., van Paradijs J., 1998, *Astrophys. J.* **500**, L101

Gallant Y. A., Achterberg A., 1999, *Mon. Not. R. Astron. Soc.* **305**, L6

Gallant Y. A., Achterberg A., Kirk J. G., 1998, in *Proc. 16th European Cosmic Ray Symposium*, p. 371, Alcalá de Henares

Gallant Y. A., Arons J., 1994, *Astrophys. J.* **435**, 230

Heavens A., Drury L'O. C., 1988, *Mon. Not. R. Astron. Soc.* **235**, 997

Hester J. J. et al., 1995, *Astrophys. J.* **448**, 240

Hjellming R. M., Rupen M. P., 1995, *Nature* **375**, 464

Hoyle F., 1960, *Mon. Not. R. Astron. Soc.* **120**, 338

Hudson P. D., 1965, *Mon. Not. R. Astron. Soc.* **131**, 23

Hudson P. D., 1967, *Mon. Not. R. Astron. Soc.* **137**, 205

Jiang D. R., Cao X., Hong X., 1998, *Astrophys. J.* **494**, 139

Jokipii J. R., 1971, *Rev. Geophys. Space Phys.* **9**, 27

Jones F. C., Ellison D. C., 1991, *Space Sci. Rev.* **58**, 259

Kennel C. F., Coroniti F. V., 1984, *Astrophys. J.* **283**, 694

Kirk J. G., 1988, *Habilitation Theses*, preprint No. 345, Max-Planck-Institut für Astrophysik, Garching

Kirk J. G., Heavens A., 1989, *Mon. Not. R. Astron. Soc.* **239**, 995

Kirk J. G., Schneider P., 1988, *Astron. Astrophys.* **201**, 177

Kirk J. G., Schneider P., 1987a, *Astrophys. J.* **315**, 425

Kirk J. G., Schneider P., 1987b, *Astrophys. J.* **322**, 256

Königl A., 1981, *Astrophys. J.* **243**, 700

Krymsky G. F., 1977, *Dokl. Akad. Nauk SSSR* **234**, 1306, (Engl. transl. Sov. Phys.-Dokl. **23**, 327)

Kulkarni S. R. et al., 1998, *Nature* **393**, 35

Lagage P. O., Cesarsky C., 1983, *Astron. Astrophys.* **125**, 249

Lieu R., Quenby J. J., Drolias B., Naidu K., 1994, *Astrophys. J.* **421**, 211

Lucek S. G., Bell A. R., 1994, *Mon. Not. R. Astron. Soc.* **268**, 581

Medvedev M. V., Loeb A., 1999, *Astrophys. J.* submitted (astro-ph/9904363)

Meegan C. A., Fishman G. J., Wilson R. B., Paciesas W. S., Pendleton G. N., Horack J. M., Brock M. N., Kouveliotou C., 1992, *Nature* **355**, 143

Mirabel I. F., Rodriguez, L. F., 1994, *Nature*, **371**, 46

Naito T., Takahara F., 1995 *Mon. Not. R. Astron. Soc.* **275**, 1077

Newman P. L., Moussas X., Quenby J. J., Valdes-Galicia J. F., Theodossiou-Ekaterinidi Z., 1992, *Astron. Astrophys.* **255**, 443

Paczynski B., Xu G., 1994, *Astrophys. J.* **427**, 708

Parker E. N., 1958, *Phys. Rev.* **109**, 1328

Quenby J. J., Drolias B., 1995, in *Proc. 24th Int. Cosmic Ray Conf.* **3**, p. 261, Rome

Quenby J. J., Lieu R., 1989, *Nature* **342**, 654

Ostrowski M., 1988, *Mon. Not. R. Astron. Soc.* **233**, 257

Ostrowski M., 1991, *Mon. Not. R. Astron. Soc.* **249**, 551

Ostrowski M., 1993, Mon. Not. R. Astron. Soc. **264**, 248
Ostrowski M., 1994, Comments Astrophys. **17**, 207
Ostrowski M., Schlickeiser R., 1996, Sol. Phys. **167**, 381
Schatzman E., 1963, Ann. Astrophys. **26**, 234
Takahara F., Terasawa T., 1990, in Proc. ICRR Int. Symp. on "Astrophysical Aspects of the Most Energetic Cosmic Rays", Kofu
Tingay S. J. et al., 1995, Nature **374**, 141
Vermeulen R. C., Cohen M. H., 1994, Astrophys. J. **430**, 467
Vietri M., 1995, Astrophys. J. **453**, 883
von Montigny C. et al., 1995, Astrophys. J. **440**, 525
Waxman E., 1995, Phys. Rev. Lett. **75**, 386
Waxman E., 1997, Astrophys. J., **485**, L5
Woods E., Loeb A., 1995, Astrophys. J. **453**, 583